© 2021. Published by The Company of Biologists Ltd | Journal of Cell Science (2021) 134, jcs250274. doi:10.1242/jcs.250274

RESEARCH ARTICLE

The protein tyrosine phosphatase PTP-PEST mediates hypoxia-induced endothelial autophagy and angiogenesis via AMPK activation

Shivam Chandel[1], Amrutha Manikandan[1], Nikunj Mehta[1,*], Abel Arul Nathan[1], Rakesh Kumar Tiwari[1], Samar Bhallabha Mohapatra[1], Mahesh Chandran[2], Abdul Jaleel[2], Narayanan Manoj[1] and Madhulika Dixit[1,‡]

ABSTRACT

Global and endothelial loss of PTP-PEST (also known as PTPN12) is associated with impaired cardiovascular development and embryonic lethality. Although hypoxia is implicated in vascular remodelling and angiogenesis, its effect on PTP-PEST remains unexplored. Here we report that hypoxia (1% oxygen) increases protein levels and catalytic activity of PTP-PEST in primary endothelial cells. Immunoprecipitation followed by mass spectrometry revealed that α subunits of AMPK (α_1 and α_2, encoded by *PRKAA1* and *PRKAA2*, respectively) interact with PTP-PEST under normoxia but not in hypoxia. Co-immunoprecipitation experiments confirmed this observation and determined that AMPK α subunits interact with the catalytic domain of PTP-PEST. Knockdown of PTP-PEST abrogated hypoxia-mediated tyrosine dephosphorylation and activation of AMPK (Thr^{172} phosphorylation). Absence of PTP-PEST also blocked hypoxia-induced autophagy (LC3 degradation and puncta formation), which was rescued by the AMPK activator metformin (500 µM). Because endothelial autophagy is a prerequisite for angiogenesis, knockdown of PTP-PEST also attenuated endothelial cell migration and capillary tube formation, with autophagy inducer rapamycin (200 nM) rescuing angiogenesis. In conclusion, this work identifies for the first time that PTP-PEST is a regulator of hypoxia-induced AMPK activation and endothelial autophagy to promote angiogenesis.

KEY WORDS: PTP-PEST, Hypoxia, AMPK, Autophagy, Angiogenesis

INTRODUCTION

Physiological hypoxia is a potent agonist for embryonic development and post-natal angiogenesis. Oxygen concentrations ranging from 1% to 5% are observed in the uterine environment between embryonic days 3.5 to 14.5 (E3.5–E14.5) to facilitate development of the placenta. Similarly, in response to hypoxia (<2% oxygen), endocardial and vascular endothelial cells mediate formation of foetal heart and vasculature, respectively, in mice between embryonic days E7.5 and E15 (Dunwoodie, 2009; Simon and Keith, 2008). Post-natal angiogenesis, as seen in the female reproductive tract during the menstrual cycle, as well as formation of collateral circulation to overcome coronary artery blocks, also depends on hypoxia-induced endothelial signalling.

Multiple studies in rodents have reported increased activity of cytosolic protein tyrosine phosphatases (PTPs) at sites of post-natal angiogenesis, including ischemic myocardium and skeletal muscles (Sugano et al., 2004; Yang et al., 2020). An increase in the cytosolic PTP activity during hypoxia is also seen in the cerebral cortex of newborn piglets (Ashraf et al., 2004). Paradoxically, others have shown that a non-selective PTP inhibitor, sodium orthovanadate, enhances VEGFR2 (also known as KDR) signalling and capillary morphogenesis (Montesano et al., 1988; Sugano et al., 2004). Although these studies allude to the involvement of different PTPs in hypoxia-induced angiogenic signalling, barring the involvement of a few, for instance VE-PTP (also known as PTPRB; a receptor PTP), the identity of hypoxia-responsive angiogenic cytosolic PTPs remains largely unknown.

Human genome encodes 38 classical PTPs, which are specific for tyrosine residues (Barr et al., 2009). Among these, PTP-PEST (also known as PTPN12) is a ubiquitously expressed cytosolic PTP with an N-terminal catalytic domain (1–300 amino acids) and a regulatory C-terminal PEST domain (301–780 amino acids), which consists of four PEST motifs. The latter plays a crucial role in protein–protein interaction, allowing the enzyme to interact with its known substrates [Cas, Paxillin, FAK (PTK2) or Pyk2 (PTK2B)], in addition to being a protein degradation signal (Davidson and Veillette, 2001; Lee and Rhee, 2019; Veillette et al., 2009). The catalytic domain harbours the conserved phosphatase 'HC[X]$_5$R' motif, surrounded by the 'WPD loop' and the 'Q loop' on one side to assist in catalysis, and by the 'P-Tyr-loop' on the other side to regulate substrate recognition and specificity (Dong et al., 2017). Both global and endothelial deficiency of PTP-PEST in mice leads to embryonic lethality between E9.5 and E10.5 due to defective heart formation and impaired endothelial network in the yolk sac (Sirois et al., 2006; Souza et al., 2012). It is worth noting that this stage in embryonic development coincides with hypoxia-induced morphogenesis (Dunwoodie, 2009; Simon and Keith, 2008). PTP-PEST appears to be crucial for vascular development even in humans, since a partial deletion of PTP-PEST is associated with disrupted aortic arch development (Duffy et al., 2015). Intriguingly, in a recent study, enhanced endothelial expression of PTP-PEST was observed in the vascularized core of glioblastoma tumours, with others demonstrating involvement of PTP-PEST in integrin-mediated endothelial cell adhesion and migration (Chen et al., 2018; Souza et al., 2012). Based on these observations, which illustrate an essential role of PTP-PEST in vascular development, and given the fact that hypoxia is indispensable for angiogenesis, in this study we set out to

[1]Department of Biotechnology, Bhupat and Jyoti Mehta School of Biosciences, Indian Institute of Technology Madras (IIT Madras), Chennai, Tamil Nadu 600036, India. [2]Cardiovascular Disease and Diabetes Biology Program, Rajiv Gandhi Centre for Biotechnology (RGCB), Thyacaud Post, Thiruvananthpuram, Kerala 695014, India.
*Present address: Howard Hughes Medical Institute and the Department of Neuroscience, University of Wisconsin, Madison, WI 53705, USA.

‡Author for correspondence (mdixit@iitm.ac.in)

S.C., 0000-0001-5034-0431; N.M., 0000-0001-7282-0428; A.A.N., 0000-0002-7203-6104; S.B.M., 0000-0002-4617-8352; M.D., 0000-0002-1898-0479

Handling Editor: John Heath
Received 18 June 2020; Accepted 23 November 2020

Journal of Cell Science (2021) 134, jcs250274. doi:10.1242/jcs.250274

determine the functional role of PTP-PEST in hypoxia-induced endothelial responses. We assessed the effect of hypoxia on the expression, activity and the binding partners of PTP-PEST in primary human umbilical vein-derived endothelial cells (HUVECs).

RESULTS

Hypoxia enhances PTP-PEST protein levels and enzyme activity

To determine the effect of hypoxia (1% oxygen) on protein levels and enzyme activity of PTP-PEST in endothelial cells, HUVECs were cultured as monolayer and exposed to hypoxia for different time points. As can be seen in Fig. 1A and summarized in Fig. 1B, immunoblotting for PTP-PEST demonstrated a significant increase in protein levels from 3 h onwards that was sustained until 24 h. Increase in protein levels of HIF-1α (also known as HIF1A) confirmed induction of hypoxia in these cells. This experiment was performed on ten biological replicates, each time with a fresh batch of HUVECs. Furthermore, to determine whether this effect of hypoxia on PTP-PEST expression is an endothelial-specific phenomenon, or is also observed in other cell types, we checked for changes in PTP-PEST expression in response to hypoxia (1% oxygen) in other cell lines, including HEK293 (n=5), HA-VSMC (human aortic vascular smooth muscle cell; n=3), HeLa (human cervical epitheloid carcinoma cell line; n=4) and Huh7 (hepatocyte derived; n=3). As seen in Fig. 1C, hypoxia promotes PTP-PEST protein expression even in other cell lines, suggesting this to be a universal phenomenon. Equal loading and induction of hypoxia were confirmed for each of the cell lines via immunoblotting for β-actin and HIF-1α, respectively (Fig. 1C). We also checked for changes in subcellular localization of PTP-PEST in response to hypoxia (1% oxygen) by immunofluorescence imaging. Cytoplasmic localization of PTP-PEST was observed in normoxia and did not alter upon hypoxia (1%

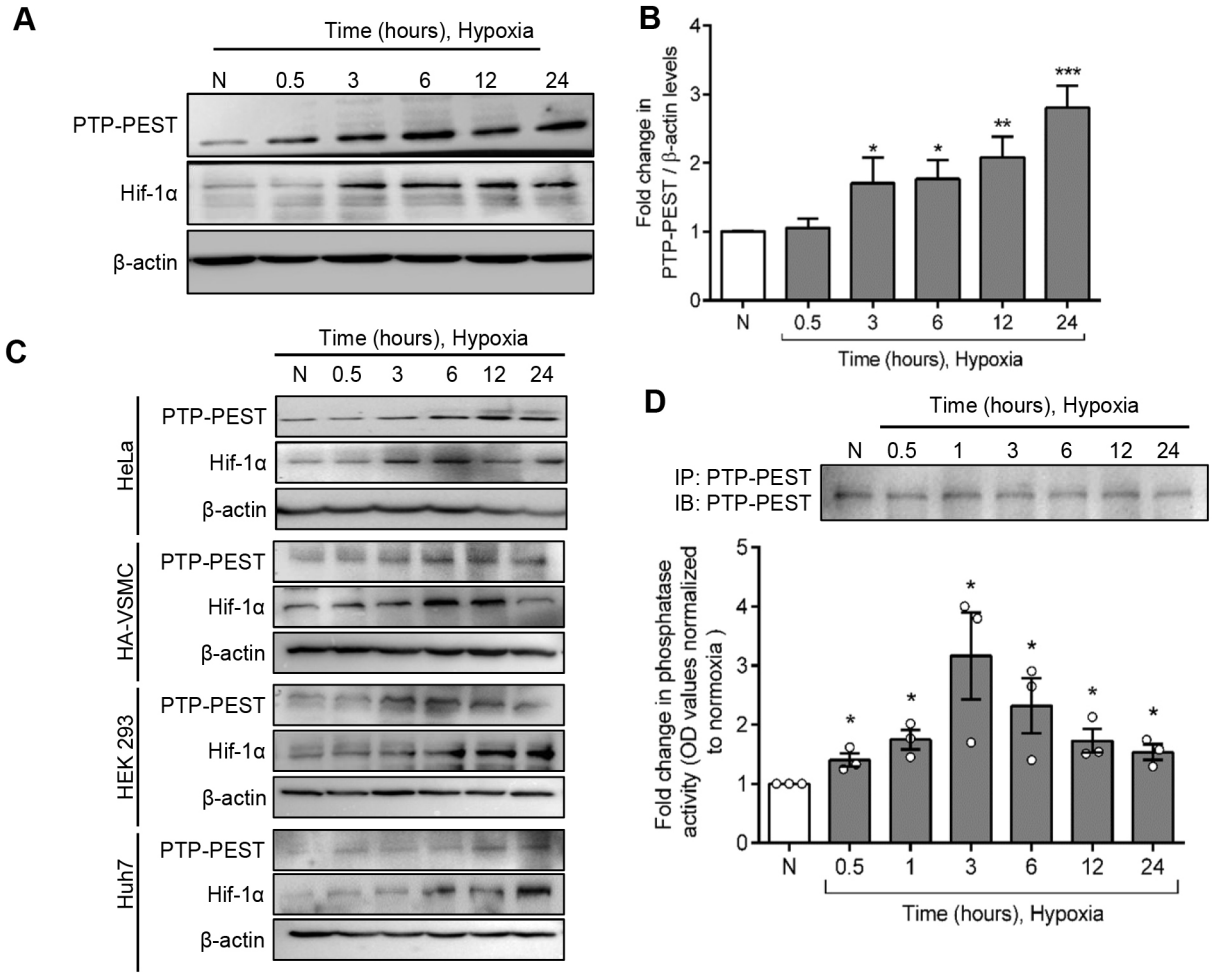

Fig. 1. Hypoxia induces an increase in protein level and enzyme activity of PTP-PEST. (A) Representative western blot image demonstrating an increase in protein levels of PTP-PEST in HUVECs exposed to hypoxia (1% O_2) for different durations. Induction of hypoxia was confirmed by western blotting for Hif-1α, and β-actin blots confirmed equal protein loading. The immunoblots represent data from ten independent experiments, with each experiment performed using a fresh batch of primary endothelial cells. N, normoxia sample. (B) Bar graph summarizing fold change in PTP-PEST to β-actin densitometry ratio, as mean±s.e.m. relative to normoxia, for western blots performed on ten independent experiments. (C) Representative western blots demonstrating expression of PTP-PEST, HIF-1α and β-actin in response to hypoxia (1% O_2) in HeLa (n=4), HA-VSMC (n=3), HEK293 (n=5) and Huh7 (n=3) cell lines. (D) Bar graph summarizing mean±s.e.m. changes in catalytic activity of endogenous PTP-PEST in response to hypoxia compared with normoxia in HUVECs for three independent experiments. Following hypoxia (1% O_2) treatment, equal amounts of PTP-PEST were immunoprecipitated from HUVEC lysates with the aid of an anti-PTP-PEST monoclonal antibody. An *in vitro* phosphatase assay was performed on the immunoprecipitated enzyme, and catalytic activity was determined through colorimetry as the amount of para-nitro phenol generated. Inset: representative western blot panel confirming equal pulldown of immunoprecipitated PTP-PEST. IP: immunoprecipitation, IB: immunoblotting. A bar graph confirming equal pulldown across conditions for three independent experiments is shown in Fig. S1B. *P<0.05; **P<0.01; ***P<0.001 versus normoxia (two-tailed unpaired Student's t-test).

Journal of Cell Science (2021) 134, jcs250274. doi:10.1242/jcs.250274

oxygen) treatment (Fig. S1A). This experiment was performed thrice, each time with a new batch of HUVECs.

Since endothelial cells, by virtue of their location, are one of the early responders to changes in oxygen tension and are resilient to hypoxia to promote adaptive angiogenesis (Filippi et al., 2018; Koziel and Jarmuszkiewicz, 2017), we employed primary endothelial cells (HUVECs) as model cell system to determine the role of PTP-PEST in hypoxia-mediated cellular responses. We set out to determine whether hypoxia (1% oxygen) influences the catalytic activity of PTP-PEST. Equal amounts of endogenous PTP-PEST were immunoprecipitated from endothelial lysates taken at different time points of hypoxia treatment (Fig. 1D; Fig. S1B) and were subjected to an immunophosphatase assay. As seen in the bar graph of Fig. 1D, hypoxia induced a significant increase in phosphatase activity of PTP-PEST, with the activity being maximal at 3 h compared with normoxia treatment. Thus, hypoxia increases both protein levels and enzyme activity of PTP-PEST.

PTP-PEST interacts with AMPK α subunits

To understand the functional relevance of hypoxia-mediated enhanced expression and activity of PTP-PEST, it was necessary to recognize its binding partners. Most of the reported binding partners of PTP-PEST are involved in cell adhesion, migration and cytoskeletal reorganization (Davidson and Veillette, 2001; Lee and Rhee, 2019; Veillette et al., 2009). We wanted to identify binding partners of PTP-PEST, specifically in endothelial cells exposed to hypoxia and normoxia. For this, HUVECs were transduced with N-terminal GST-tagged PTP-PEST lentiviral particles (as described in the Materials and Methods). Post-transduction, the same pool of cells was split and exposed to either normoxia or hypoxia (1% oxygen) for 24 h. Equal amounts of GST-tagged PTP-PEST were pulled down via immunoprecipitation using an anti-GST antibody, and the co-immunoprecipitated proteins were subjected to liquid chromatography-mass spectrometry (LC/MS/MS) analysis (see Materials and Methods).

The protein IDs obtained after mass spectrometry (MS) data were filtered for non-specific binding partners by removal of proteins appearing in MS of the isotype control sample. In addition, MS contaminants, as per the common repository of adventitious proteins (https://www.thegpm.org/crap/), as well as proteins that are a part of the Sepharose bead proteome were excluded from the analysis (Trinkle-Mulcahy et al., 2008). Proteins unique only to normoxia or hypoxia were subjected to analysis using the gene ontology program PANTHER (Thomas et al., 2003). The prominent binding partners observed solely in normoxia were signalling molecules, transcription factors and cytoskeletal proteins (Fig. 2A), whereas binding partners such as chaperones, hydrolases and oxidoreductases appeared exclusively in hypoxia (Fig. 2A). Some of the specific binding partners observed in normoxia and hypoxia are listed in Fig. 2B. In hypoxia, we found proteins including OTUB1, PGK1 and PKC-ε (PRKCE), which are known to play an important role in regulating autophagy, interacting with PTP-PEST. Surprisingly, proteomic studies revealed AMPK α_1 and α_2 (encoded by *PRKAA1* and *PRKAA2*, respectively), the catalytic subunits of 5′-AMP-activated protein kinase (AMPK), as interacting partners of PTP-PEST in normoxia (Fig. 2B). Co-immunostaining of PTP-PEST and AMPK α subunits (referred to hereafter as AMPKα) followed by confocal immunofluorescence imaging demonstrated that both PTP-PEST and AMPKα indeed colocalize in the cytoplasm of HUVECs (Fig. 2C).

Intriguingly, our proteomics data revealed that interaction of PTP-PEST with AMPKα was lost upon hypoxia treatment. In order to validate the interaction of PTP-PEST with AMPKα, we performed co-immunoprecipitation experiments. Equal amounts of endogenous PTP-PEST were pulled down from normoxia- and hypoxia (1% oxygen, 24 h)-exposed HUVECs and immunoblotting was performed for AMPKα. It is worth noting that the anti-AMPKα antibody used for immunoblotting recognizes both α_1 and α_2 isoforms of the α subunit. In accordance with the proteomics data, we found interaction of PTP-PEST with AMPKα in normoxic conditions; however, this interaction was abrogated in HUVECs exposed to hypoxia (1% oxygen) for 24 h (Fig. 3A). Equal pulldown of PTP-PEST across the two conditions was confirmed by re-probing the blot for PTP-PEST. This experiment was performed four independent times, each time with a different batch of HUVECs.

PTP-PEST consists of an N-terminal catalytic domain and a long C-terminal non-catalytic domain, rich in PEST sequences. The C-terminal domain plays a significant role in regulating the enzyme activity of PTP-PEST by facilitating its interaction with either substrates and/or other adaptor proteins (Davidson and Veillette, 2001; Lee and Rhee, 2019; Veillette et al., 2009). Next, we checked whether the PEST domain is also essential for the interaction of PTP-PEST with AMPKα. We cloned the His-tagged wild type (WT) and enzymatically inactive (C231S) N-terminal catalytic domain (1–300 amino acids) lacking the C-terminal PEST sequences of human PTP-PEST into the pET28a(+) bacterial expression vector. The two proteins were overexpressed and purified from the *E. coli* BL21 codon plus RIL (DE3) strain (Fig. S2A–C). A total of 100 µg of purified WT and C231S mutant PTP-PEST protein lacking the PEST motifs were independently incubated with 500 µg of HUVEC lysate for 8 h at 4° C. This was followed by immunoprecipitation of PTP-PEST using an anti-His-tag antibody and immunoblotting for AMPKα (Fig. 3B). Equal pulldown of PTP-PEST was confirmed by re-probing the blot for PTP-PEST. We found co-immunoprecipitation of AMPKα with the N-terminal catalytic domain of PTP-PEST (Fig. 3B), which suggests that the interaction of AMPKα with PTP-PEST is not dependent on the C-terminal PEST domain. Moreover, co-immunoprecipitation of AMPKα with the C231S (catalytically inactive) mutant was greater in comparison to that with WT (Fig. 3B), despite equal pulldown of PTP-PEST protein across the two conditions, suggesting that AMPKα is a likely substrate of PTP-PEST. This experiment was performed thrice, each time with a fresh batch of HUVECs.

PTP-PEST mediates hypoxia-induced AMPK activation

AMPK is a heterotrimeric stress responsive serine-threonine kinase known to play an important role in maintaining cellular energy homeostasis as well as autophagy (Jeon, 2016). Next, we wanted to understand the relevance of the interaction of AMPKα subunit with PTP-PEST, a tyrosine phosphatase. Since PTP-PEST interacts with AMPKα via its catalytic domain, we were interested in examining whether PTP-PEST can dephosphorylate AMPKα. First, we determined the effect of hypoxia on total tyrosine phosphorylation of AMPKα. We initially tried immunoprecipitating endogenous AMPKα but faced some difficulties. Hence, we resorted to an alternative approach that was employed by Yamada et al. (2016). For this, HUVECs were exposed to hypoxia (1% oxygen) for different time periods. Equal amounts of HUVEC lysate (300 µg) following experimental treatment were subjected to immunoprecipitation with 3 µg of anti-phospho-tyrosine antibody, followed by immunoblotting for AMPKα. Tyrosine phosphorylation of AMPKα in HUVECs exposed to hypoxia for 24 h was lower in comparison to that in HUVECs exposed to normoxia (Fig. 3C), indicating

Journal of Cell Science (2021) 134, jcs250274. doi:10.1242/jcs.250274

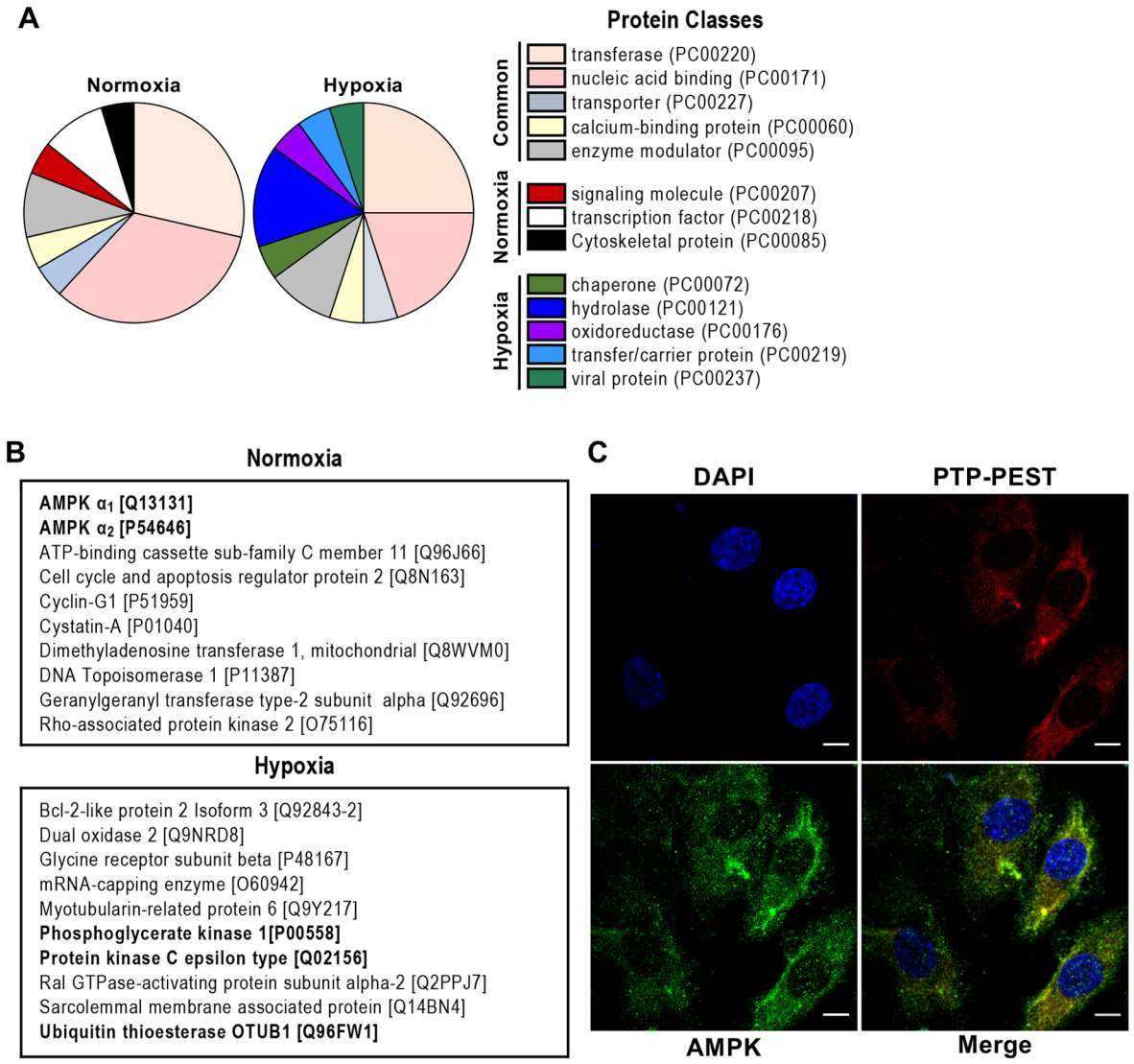

Fig. 2. Identification of binding partners of PTP-PEST under normoxia and hypoxia in HUVECs through LC/MS/MS-based proteomics and proteomic data analysis. (A,B) Following mass spectrometry of immunoprecipitated PTP-PEST, proteins unique to normoxia or hypoxia were subjected to analysis by the gene ontology program PANTHER (Thomas et al., 2003). (A) Pie chart representing classes of interacting protein partners of PTP-PEST in normoxia and hypoxia. IDs of protein classes as annotated by PANTHER are listed in parentheses. (B) List of some of the proteins interacting with PTP-PEST exclusively either in normoxia or in hypoxia. Uniprot IDs of binding proteins are listed in parentheses. (C) Representative confocal immunofluorescence images demonstrating colocalization of PTP-PEST and AMPKα in HUVECs, representative of three independent experiments, with each experiment performed on a fresh batch of HUVECs. Co-immunostaining was performed for PTP-PEST (red) and AMPKα (green) to demonstrate their colocalization in HUVECs. Nuclei were stained with DAPI. Scale bars: 10 µm.

dephosphorylation of AMPKα. It is worth noting that the total AMPKα levels in endothelial cells did not change across treatment conditions (Fig. 3C). The experiment was performed in n=4 biological replicates, each time with a different batch of HUVECs.

Next, we knocked down PTP-PEST using shRNA lentivirus to check its effect on AMPKα tyrosine dephosphorylation in response to hypoxia (1% oxygen, 24 h). Scrambled shRNA lentivirus was used as negative control. We found that hypoxia-induced AMPKα dephosphorylation was indeed abrogated upon PTP-PEST knockdown (Fig. 3D,E). In fact, in the absence of PTP-PEST, the basal tyrosine phosphorylation of AMPKα itself was increased, whereas the total protein levels of AMPKα remained unchanged upon PTP-PEST knockdown. Successful knockdown of PTP-PEST was confirmed through western blotting, as seen in Fig. 3D. Thus, three independent experiments confirmed that PTP-PEST does regulate tyrosine dephosphorylation of AMPKα in response to hypoxia without influencing AMPKα protein levels.

AMPK can be regulated both allosterically and by means of posttranslational modifications. Phosphorylation at Thr^{172} residing in the kinase domain of the α subunit is an efficient mechanism of AMPK activation (Jeon, 2016). Therefore, next, the effect of hypoxia on AMPK activation in endothelial cells was examined. HUVECs were exposed to hypoxia for different time points, and immunoblotting was performed for phosphorylation of Thr^{172}. Thr^{172} phosphorylation was seen in response to hypoxia as early as 15 min and was sustained up to 24 h (Fig. 3F; Fig. S2D) for five independent experiments. Since we observed that PTP-PEST mediates hypoxia-induced tyrosine dephosphorylation of AMPK, we set out to determine if absence of PTP-PEST also influences Thr^{172} phosphorylation of AMPK. For this purpose, HUVECs were transduced with PTP-PEST shRNA and

Journal of Cell Science (2021) 134, jcs250274. doi:10.1242/jcs.250274

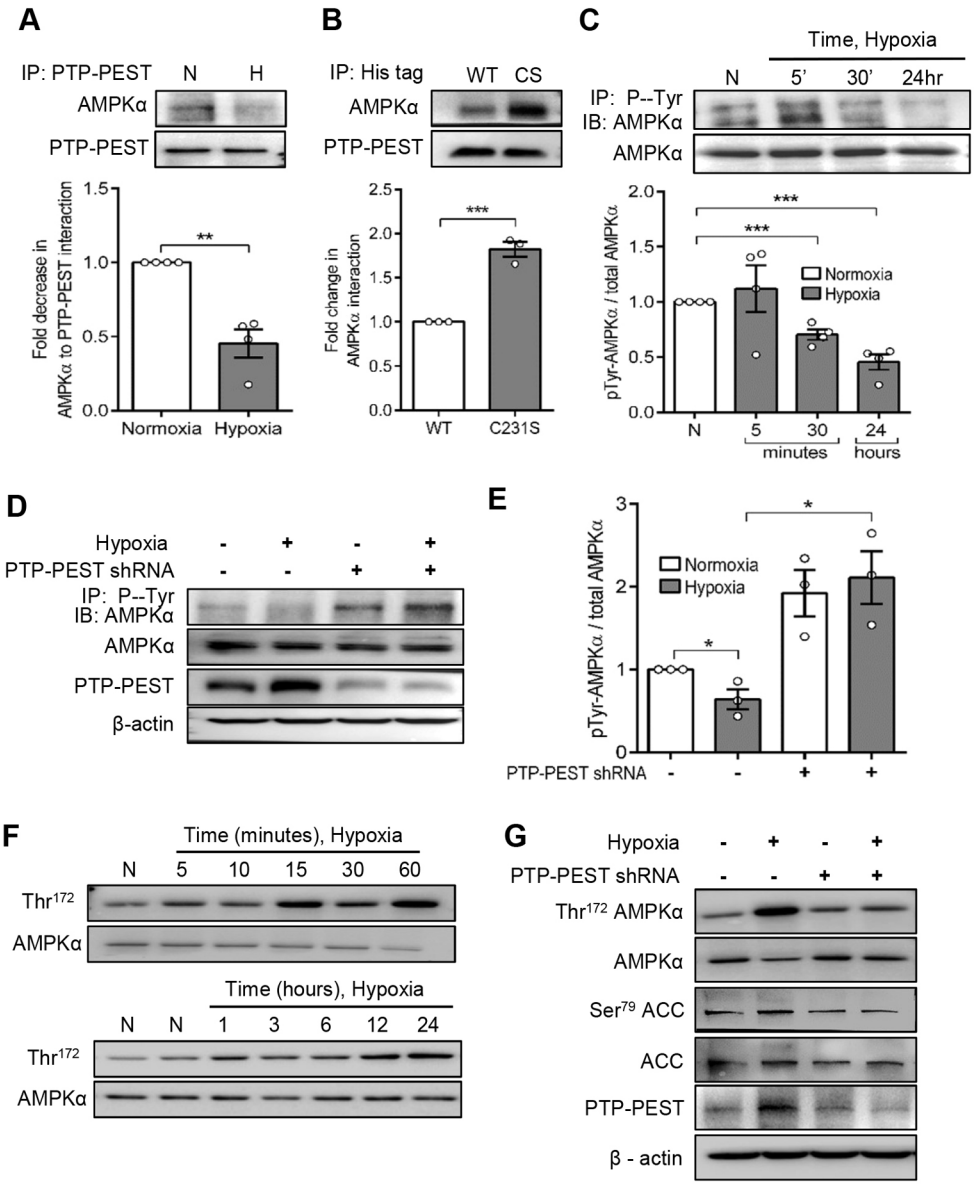

Fig. 3. AMPKα is an interacting partner and substrate of PTP-PEST. (A) Representative western blot and bar graph depicting co-immunoprecipitation of AMPKα with PTP-PEST from HUVECs exposed to 24 h of hypoxia (H; 1% O_2) and normoxia (N). Endogenous PTP-PEST was immunoprecipitated from HUVECs exposed to either normoxia or hypoxia and was subjected to western blotting. Probing of blots for AMPKα confirmed interaction of AMPKα with PTP-PEST under normoxic conditions, which was decreased for hypoxia-treated cells. Re-probing of blots with anti-PTP-PEST antibody confirmed equal pulldown of PTP-PEST. Bar graph summarizes the fold decrease in densitometric ratio of AMPKα to PTP-PEST observed under hypoxia, relative to the ratio in normoxia-treated cells. Data presented are the mean±s.e.m. of four independent experiments. (B) Representative western blot and bar graph showing co-immunoprecipitation of endogenous AMPKα with His-tagged PTP-PEST when equal amounts of HUVEC lysate (500 µg) were treated with equal amounts (100 µg) of either purified His-tagged WT or C231S mutant (CS) PTP-PEST (1–300 amino acids). Immunoprecipitation of PTP-PEST was performed with 1 µg anti-His-tag antibody, and interaction of AMPKα was confirmed through western blotting of immunoprecipitated proteins. This experiment was performed thrice, each time with a fresh batch of primary endothelial cells. Bar graph summarizes data as mean±s.e.m. fold change in interaction of AMPKα with PTP-PEST, normalized to the AMPKα to WT PTP-PEST ratio. (C) Representative western blot demonstrating the effect of hypoxia on AMPKα tyrosine dephosphorylation for four independent experiments. Following experimental treatment of hypoxia (1% O_2), HUVEC cell lysate was subjected to immunoprecipitation with anti-phospho-tyrosine antibody (P-Tyr), and the immunoprecipitated proteins were resolved using SDS-PAGE. This was followed by immunoblotting for AMPKα. Bar graph shows mean±s.e.m. phospho-tyrosine AMPKα to total AMPKα ratio across treatment conditions, normalized to the ratio in normoxia conditions, for four independent experiments, each performed on a fresh batch of HUVECs. (D) Representative western blot demonstrating effect of PTP-PEST knockdown (PTP-PEST shRNA) on hypoxia-induced AMPKα tyrosine dephosphorylation in HUVECs. Hypoxia (1% O_2) treatment was for 24 h. β-actin is shown as a loading control. (E) Bar graph summarizing the effect of PTP-PEST knockdown on hypoxia-induced AMPKα tyrosine dephosphorylation as the mean±s.e.m. phospho-tyrosine AMPKα to total AMPKα ratio, relative to normoxia-treated cells without knockdown, for three independent experiments. (F) Representative western blot depicting the effect of hypoxia on AMPKα activation (Thr^{172} phosphorylation) in HUVECs for five independent experiments. (G) Representative western blot depicting effect of PTP-PEST knockdown on hypoxia-induced AMPK (Thr^{172} phosphorylation, n=5) and ACC (Ser^{79} phosphorylation, n=3) activation. Knockdown of PTP-PEST in HUVECs was achieved through lentivirus-mediated expression of PTP-PEST shRNA, which was confirmed for each of the experiments using western blotting. Western blotting for the corresponding proteins confirmed no changes in protein levels of AMPKα and ACC. β-actin is shown as a loading control. Each independent experiment was performed with a different batch of primary endothelial cells (HUVECs). IP, immunoprecipitation; IB, immunoblotting. *P<0.05; **P<0.01; ***P<0.001 (two-tailed unpaired Student's t-test).

scrambled shRNA lentivirus followed by hypoxia treatment (1% oxygen, 24 h) and immunoblotting for phospho-Thr^{172} AMPKα. Interestingly, we found that hypoxia-induced AMPK activation was attenuated in HUVECs upon PTP-PEST knockdown (Fig. 3G). Simultaneously, we also checked for phosphorylation of ACC at Ser^{79} (acetyl-CoA carboxylase, a known substrate of AMPK) as a readout of AMPK activity. We found that hypoxia-induced phosphorylation of ACC at Ser^{79} was also attenuated in PTP-PEST knockdown cells (Fig. 3G). These observations, in conjunction with loss of interaction between PTP-PEST and AMPKα under hypoxia, demonstrate that AMPKα is a substrate of PTP-PEST, wherein PTP-PEST mediates tyrosine dephosphorylation of AMPKα and regulates its catalytic activity.

PTP-PEST regulates hypoxia-induced autophagy via AMPK

AMPK is known to regulate autophagy via dual mechanisms involving inactivation of mTORC1 and direct phosphorylation of ULK1 at Ser^{317} (Alers et al., 2012; Kim et al., 2011). Because we observed that PTP-PEST-dependent tyrosine dephosphorylation of AMPKα is associated with its activation in response to hypoxia, we next wanted to understand the role of PTP-PEST in hypoxia-induced endothelial cell autophagy. For this, we first tested the effect of hypoxia on endothelial autophagy followed by knockdown experiments. HUVECs exposed to hypoxia (1% oxygen) for different time intervals displayed an increase in LC3 (here referring to MAP1LC3A and MAP1LC3B) degradation (LC3II form) following hypoxia (Fig. S3A,B). An increase in abundance of the LC3II form indicates induction of autophagy, because it plays an indispensable role in autophagosome biogenesis. Along with an increase in LC3II levels, other autophagic markers like beclin-1 and phosphorylation of ULK1 at Ser^{317} were also enhanced in response to hypoxia (Fig. S3A,C,D). In addition, a decrease in ULK1 Ser^{757} phosphorylation, another indicator of autophagy, was observed (Fig. S3A,E). It should be noted that Ser^{757} dephosphorylation of ULK1 reflects inactivation of mTORC1 (Kim et al., 2011). We also examined LC3 puncta formation in response to hypoxia using LC3 immunostaining followed by confocal imaging. As seen in Fig. S3F, high accumulation of LC3 puncta representing autophagosomes was observed in HUVECs treated with hypoxia (1% oxygen, 24 h). This led to a significant increase in the number of puncta per cell, as well as in the percentage of LC3-positive cells (Fig. S3G,H). Treatment with bafilomycin A1 (100 nM) further increased the number of LC3 puncta per cell, indicating that autophagy was in progress during hypoxia. Bafilomycin A1 treatment was given for the last 6 h of hypoxia treatment. These experiments were performed thrice, each time with a new batch of HUVECs.

Next, we wanted to determine whether hypoxia-induced autophagy was dependent on PTP-PEST-mediated AMPK activation. As seen in Fig. 4A,B, hypoxia (1% oxygen, 24 h)-induced LC3 degradation was significantly attenuated upon knockdown of PTP-PEST in five independent experiments. Further, we performed LC3 immunostaining in scrambled and PTP-PEST shRNA-treated endothelial cells in the absence and presence of the AMPK activator metformin (500 µM). Metformin treatment was given for 24 h along with hypoxia. As can be seen in Fig. 4C–E, the hypoxia-induced increase in the number of LC3 puncta per cell, as well as in the percentage of cells with puncta-like structures, was significantly attenuated upon PTP-PEST knockdown. This attenuation in autophagy due to the absence of PTP-PEST was, however, recovered upon metformin treatment, leading us to conclude that PTP-PEST is necessary for hypoxia-induced autophagy via AMPK activation. These experiments were repeated thrice, each time with a fresh batch of HUVECs.

PTP-PEST regulates hypoxia-induced angiogenesis via autophagy

Hypoxia, the principal physiological stimulus for angiogenesis, regulates multiple steps of sprouting angiogenesis including endothelial cell migration, tube formation and vessel branching (Forsythe et al., 1996; Krock et al., 2011; Rankin et al., 2008). Additionally, induction of autophagy in response to hypoxia is both a protective survival mechanism as well as an inducer of angiogenesis in endothelial cells (Du et al., 2012; Liang et al., 2018). We thus examined the effect of PTP-PEST knockdown on hypoxia-induced angiogenic responses such as migration and capillary tube formation. As seen in Fig. 5A and B, both basal and hypoxia (1% oxygen, 24 h)-induced endothelial cell migration was attenuated in PTP-PEST knockdown cells in wound healing experiments. Scrambled shRNA lentivirus was used as a mock transduction. The knockdown of endogenous PTP-PEST was confirmed through western blotting (Fig. 5C). This experiment was repeated four times, each time with a fresh batch of endothelial cells.

To examine the role of PTP-PEST in hypoxia-induced tube formation *in vitro*, HUVECs (15×10^3 cells) were placed on growth factor-free Matrigel in low serum (1% FBS) MCDB 131-based endothelial growth medium after transduction with scrambled shRNA or PTP-PEST shRNA lentivirus, and tube formation was allowed under normoxic and hypoxic (1% oxygen) conditions. The tubular network (Fig. 6A) was quantified after 16 h of incubation using ImageJ software. We observed an increase in the number of segments (Fig. 6C), number of junctions (Fig. 6D) and the total length of tubes (Fig. 6E) in response to hypoxia (1% oxygen). Among these effects of hypoxia, PTP-PEST knockdown significantly attenuated the number of segments and junctions. PTP-PEST knockdown was confirmed through western blotting (Fig. 6B). Interestingly, use of rapamycin (200 nM), an mTOR inhibitor and autophagy inducer, reversed the effect of loss of PTP-PEST during hypoxia by increasing the number of segments (Fig. 6A,C) and junctions (Fig. 6A,D) of tubes for PTP-PEST-knockdown cells. These experiments were repeated four times, each time with a different batch of HUVECs. Taken together, these observations indicate that PTP-PEST promotes hypoxia-induced angiogenesis through the AMPK-dependent autophagy pathway.

DISCUSSION

The results of this study demonstrate that hypoxia increases the expression and catalytic activity of the cytosolic protein tyrosine phosphatase PTP-PEST to promote endothelial autophagy and consequent angiogenesis. These functional effects of hypoxia are dependent on PTP-PEST-mediated tyrosine dephosphorylation and activation of AMPK.

As the name suggests, AMPK is a physiological energy sensor that is activated in response to increased intracellular concentrations of AMP under stress conditions of hypoxia, calorie restriction or exercise. Upon activation, it inhibits energy-utilizing anabolic processes and instead promotes catabolic processes such as fatty acid oxidation, glycolysis and autophagy (Jeon, 2016; Long and Zierath, 2006). AMPK holoenzyme is a heterotrimeric complex composed of a catalytic α subunit in complex with two regulatory subunits, β and γ (Ross et al., 2016). Binding of AMP molecules to the γ subunits during stress mediates allosteric activation of the catalytic domain of the α subunits. The kinase domain (KD) of the α subunit harbours the Thr^{172} residue in the catalytic cleft formed by its N- and C-terminal lobes (Fig. 7) (Stein et al., 2000; Woods et al., 2003). In an inactive state, the back end of these lobes opposite to the catalytic cleft are held by the evolutionarily conserved auto-inhibitory domain (AID). The AID in turn is connected to a flexible

Journal of Cell Science (2021) 134, jcs250274. doi:10.1242/jcs.250274

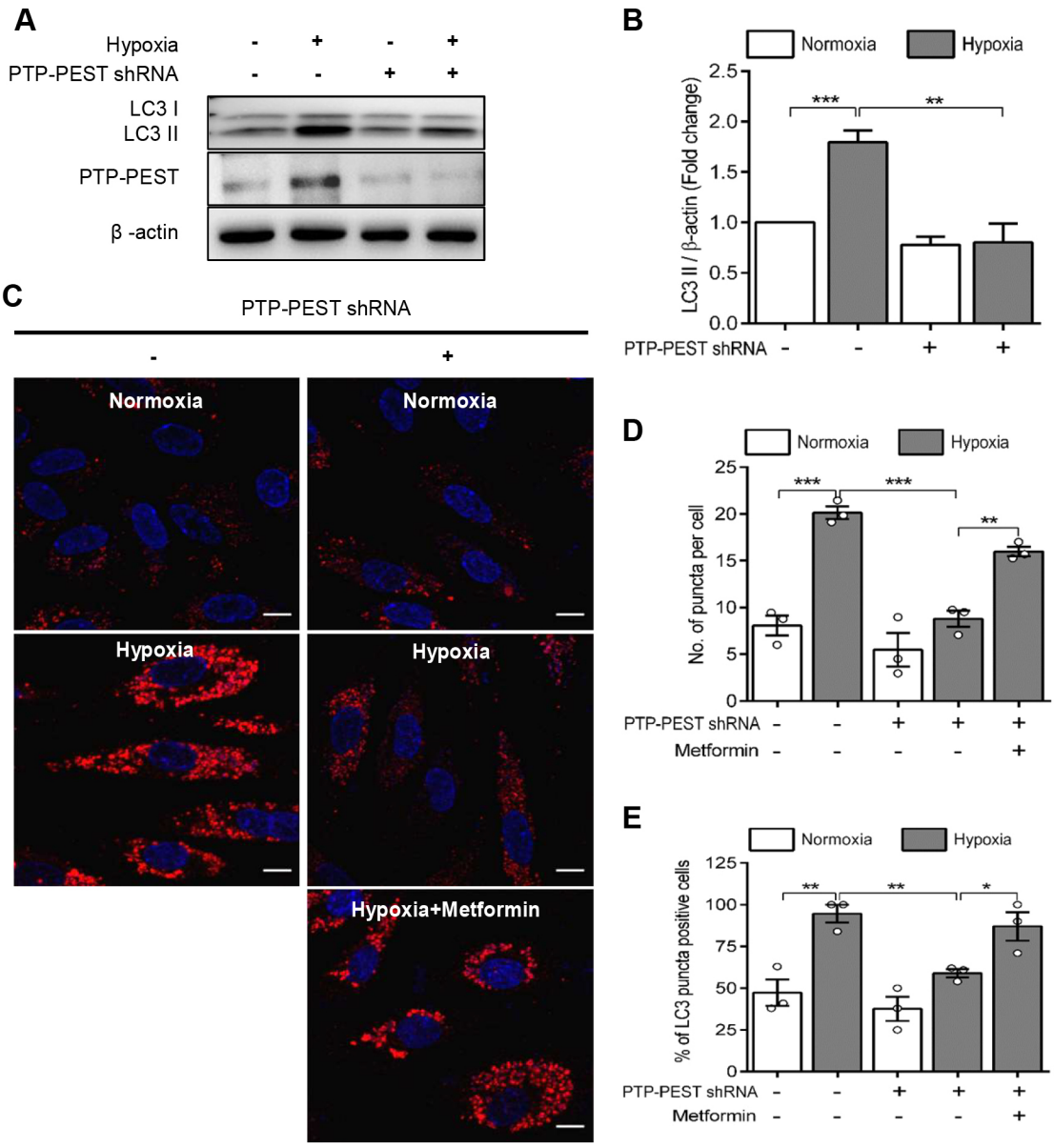

Fig. 4. Hypoxia-induced autophagy is dependent on PTP-PEST. (A) Representative western blot depicting effect of PTP-PEST knockdown on hypoxia-induced LC3 degradation (LC3 II) in HUVECs. PTP-PEST was knocked down in HUVECs through lentivirus-mediated expression of PTP-PEST shRNA. Cells were subsequently exposed to normoxia or hypoxia (1% O_2) for 24 h. (B) Bar graph summarizing fold change in LC3II to β-actin densitometric expression ratio relative to control condition (HUVECs exposed to normoxia) as mean±s.e.m. for five biological replicates. Each experiment was performed using a fresh batch of HUVECs. (C) Representative confocal immunofluorescence images demonstrating the effect of PTP-PEST knockdown on LC3 puncta formation post 24 h of normoxia, hypoxia (1% O_2) or hypoxia (1% O_2) in the presence of AMPK activator metformin (500 µM). Immunostaining was performed with LC3 antibody (red) to determine LC3 puncta formation. Nuclei were stained with DAPI (blue). Scale bars: 10 µm. (D) Bar graph summarizing data for number of puncta per cell in the indicated conditions as mean±s.e.m. for three independent experiments, with each experiment performed using a fresh batch of HUVECs. (E) Bar graph summarizing data for percentage of cells with puncta-like structures in the indicated conditions as mean±s.e.m. for three independent experiments. *P<0.05; **P<0.01; ***P<0.001 (two-tailed unpaired Student's t-test).

regulatory motif termed the α-regulatory subunit-interacting motif (α-RIM). Multiple crystallography studies have demonstrated that conformational changes in the α-RIM promote pulling of the AID away from the kinase domain to relieve inhibition (Fig. 7) (Chen et al., 2009; Li et al., 2017). As a consequence of this pulling away, Thr^{172} at the catalytic site becomes accessible for phosphorylation by LKB1 (also known as STK11) or CAMKKβ (also known as CAMKK2) to enhance AMPK enzyme activity several hundredfold (Hawley et al., 2005; Woods et al., 2003). Two isoforms of α subunit (α_1 and α_2), which exhibit considerable sequence identity and conformational similarity, have been reported (Calabrese et al., 2014). It is worth noting that both these isoforms of α subunit interacted with PTP-PEST under normoxic conditions, with the interaction being lost in hypoxia. Interestingly, both these isoforms of α subunit are expressed in endothelial cells, where they participate in hypoxia-induced angiogenesis (Davis et al., 2006; Nagata et al., 2003).

In the current study, it was found that hypoxia-induced activation of AMPK was dependent on PTP-PEST. The catalytic domain of PTP-PEST (1–300 amino acids) was sufficient for interaction with

Journal of Cell Science (2021) 134, jcs250274. doi:10.1242/jcs.250274

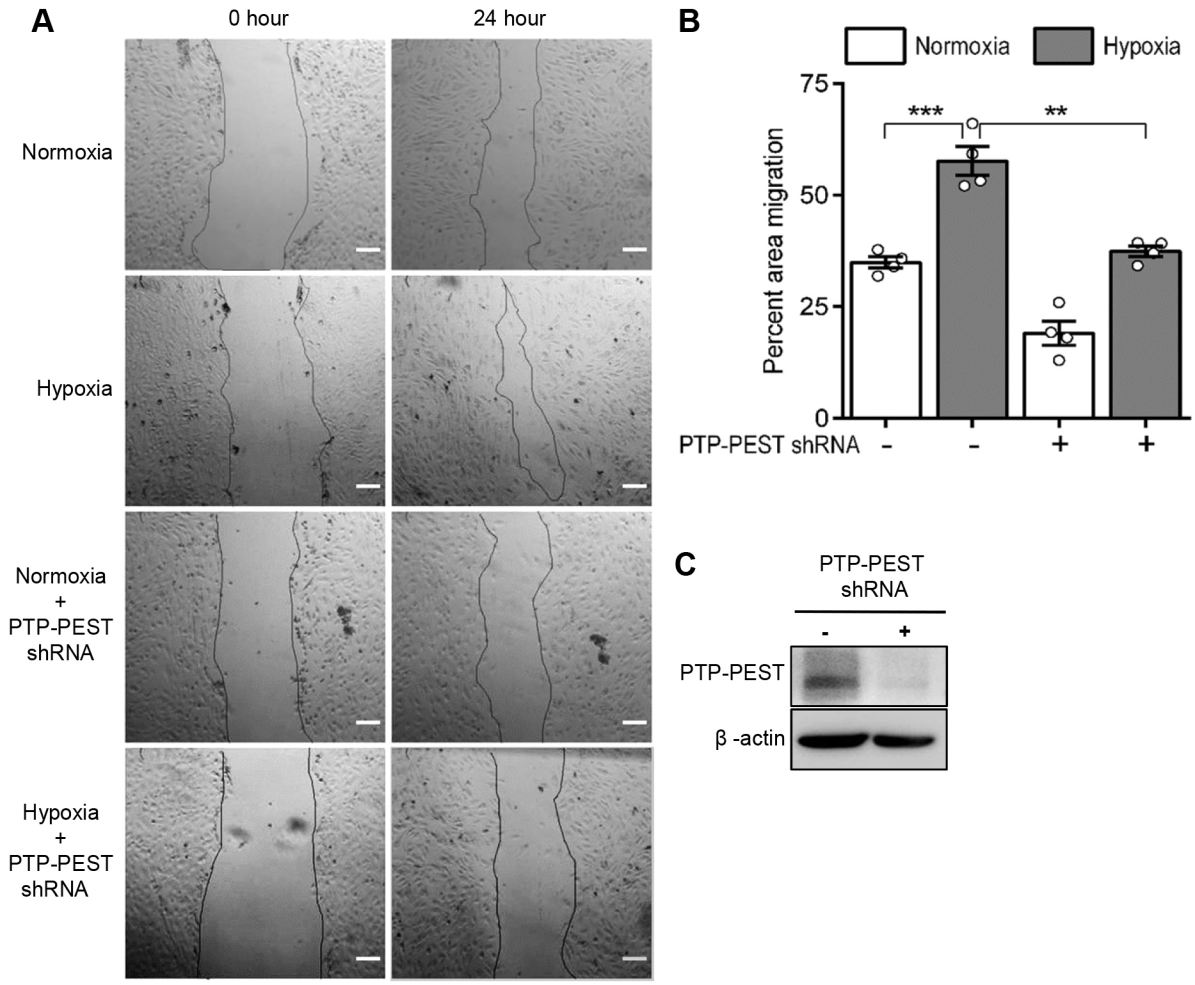

Fig. 5. Hypoxia-induced endothelial cell migration is PTP-PEST dependent. (A) Representative images of scratch wound assay demonstrating the effect of PTP-PEST knockdown (PTP-PEST shRNA) on hypoxia-induced migration of endothelial cells towards wound closure post 24 h hypoxia (1% O_2). Lines indicate the boundaries of the wound under different treatment conditions. Scale bars: 200 µm. (B) Bar graph summarizing wound closure data as percentage closure of the wound area (percent area migration) for the indicated experimental conditions, presented as mean±s.e.m. of four independent experiments. (C) Representative western blot confirming knockdown of PTP-PEST in HUVECs used for migration assays versus control cells that received scrambled shRNA. ***P*<0.01; ****P*<0.001 (two-tailed unpaired Student's *t*-test).

AMPKα, thereby suggesting that AMPKα subunits are PTP-PEST substrates. The endogenous interaction between AMPKα and PTP-PEST was lost in hypoxia. This loss of interaction coincided with tyrosine dephosphorylation of AMPKα. Interestingly, knockdown of PTP-PEST not only enhanced the basal tyrosine phosphorylation of AMPK, but also prevented hypoxia-mediated activation of AMPK, as assessed through Thr^{172} phosphorylation. To the best of our knowledge, this is the first study to directly demonstrate regulation of AMPK activity by a cytosolic protein tyrosine phosphatase. Although not much is known about the regulation of AMPK by tyrosine phosphorylation, a recent study demonstrated that phosphorylation of Tyr^{436} in the α-subunit (Fig. 7) reduces AMPK catalytic activity by modulating the AID–αRIM interaction (Yamada et al., 2016). It is thus tempting to speculate that PTP-PEST may dephosphorylate this residue of the α-subunit under hypoxic conditions to activate AMPK by inducing a conformational change in the flexible α-RIM domain to relieve auto-inhibition imparted by AID (Fig. 7). This possibility, however, needs to be examined in future studies.

One of the major consequences of AMPK activation in endothelial cells is induction of autophagy to promote survival and angiogenesis (Filippi et al., 2018; Jeon, 2016; Long and Zierath, 2006; Stempien-Otero et al., 1999). This adaptive response imparts resilience to endothelial cells towards stress conditions such as heat shock, hypoxia, shear stress and calorie restriction (De Meyer et al., 2015; Jiang, 2016; Nussenzweig et al., 2015). In fact, defective endothelial autophagy is associated with vascular aging, thrombosis, atherosclerosis and even arterial stiffness (Jiang, 2016; Xie et al., 2011). AMPK activates autophagy either by phosphorylating ULK1 at Ser^{317} or by inhibiting mTORC1 (Alers et al., 2012; Kim et al., 2011). Both these events lead to autophagosome formation. To couple the changes in PTP-PEST and AMPK activity with endothelial cell function, we assessed the consequence of PTP-PEST knockdown on hypoxia-induced autophagy. We found that despite induction of hypoxia, autophagy was attenuated in the absence of PTP-PEST. This effect was, however, rescued by the AMPK activator metformin, demonstrating that AMPK activation lies downstream of PTP-PEST in hypoxia-induced endothelial signalling. It is worth noting that metformin treatment also promotes endothelial migration and angiogenesis in experimental models of hypoxia such as stroke (Bakhashab et al., 2018; Jin et al., 2014; Nagata et al., 2003; Venna et al., 2014). Thus, AMPK is indispensable for both autophagy and angiogenesis. Likewise, we have identified an essential role of PTP-PEST in hypoxia-induced AMPK activation, autophagy and

Journal of Cell Science (2021) 134, jcs250274. doi:10.1242/jcs.250274

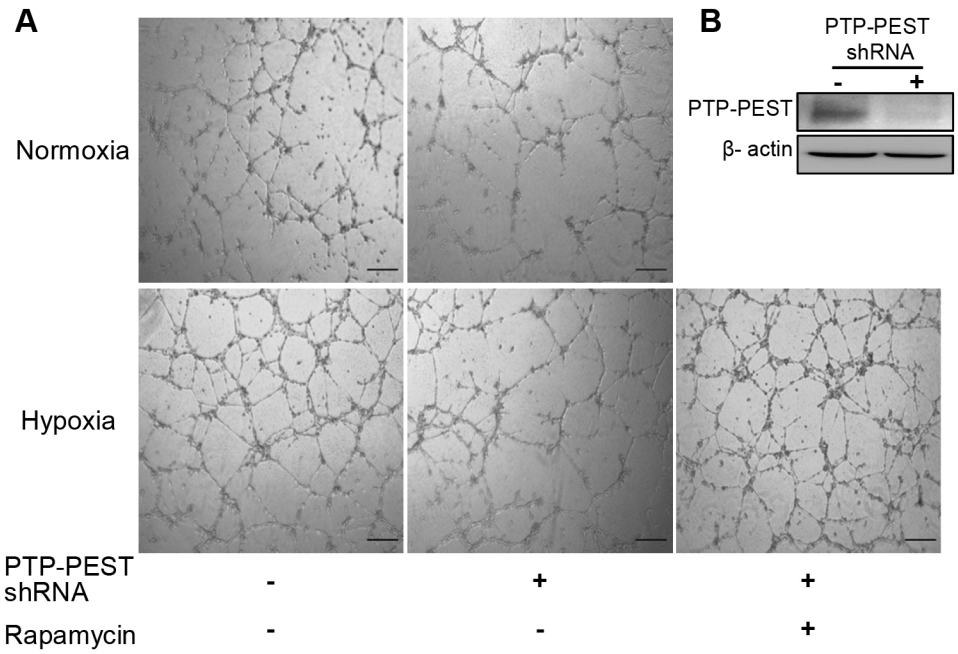

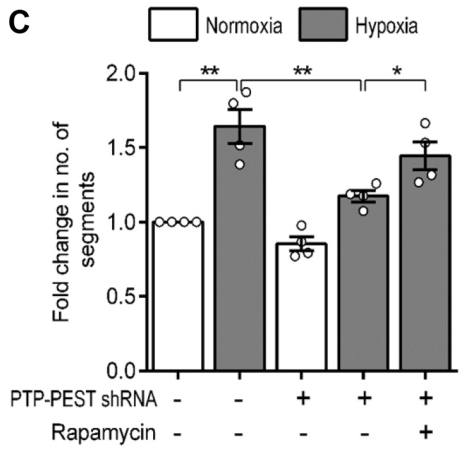

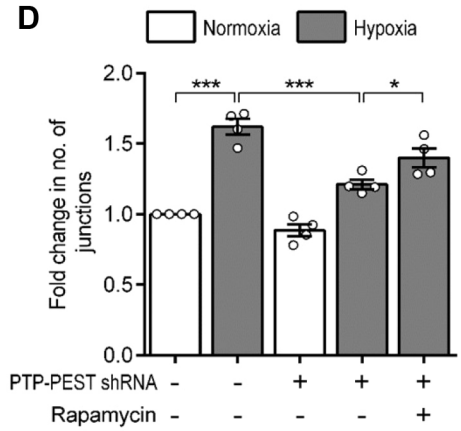

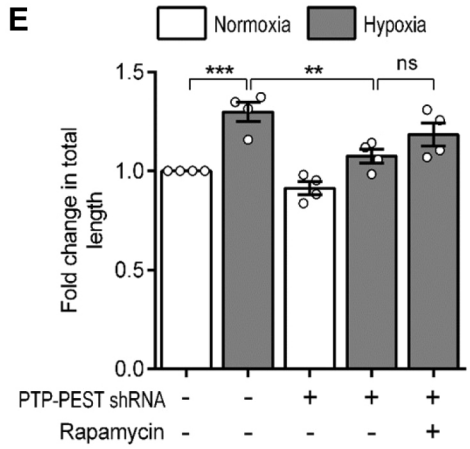

Fig. 6. Hypoxia-induced endothelial tube formation is PTP-PEST dependent. (A) Representative Matrigel images demonstrating the effect of PTP-PEST knockdown (PTP-PEST shRNA) on endothelial tube formation in the presence or absence of the autophagy inducer rapamycin (200 nM) in response to 16 h hypoxia (1% O_2). HUVECs (with or without PTP-PEST knockdown) were seeded onto Matrigel-coated wells in low serum (1% FBS) MCDB 131-based endothelial growth medium, followed by incubation under normoxia or hypoxia (1% O_2) and images were taken after 16 h of incubation. Control cells were transduced with scrambled shRNA lentivirus. Scale bars: 250 µm. (B) Representative western blot confirming PTP-PEST knockdown in HUVECs. β-actin is shown as a loading control. (C–E) Bar graphs summarizing tube formation data as mean±s.e.m. fold change relative to the control condition (normoxia, no knockdown or rapamycin) in number of segments and/or tubes (C), number of junctions (D) and length of tubes (E) for four independent experiments. Each experiment was performed using a fresh batch of HUVECs. Images were analysed using the Angioanalyser feature of ImageJ. **P*<0.05; ***P*<0.01; ****P*<0.001 (two-tailed unpaired Student's *t*-test).

consequent angiogenesis. It is interesting to note that apart from activating AMPK, PTP-PEST also interacted with other proteins including ubiquitin thioesterase (OTUB1), PKC-ε, myotubularin-related protein 6 (MTMR6) and sarcolemmal membrane-associated protein (SLMAP), all of which are either directly involved in autophagy or its regulation (Lakshmanan et al., 2016; Mochizuki

Journal of Cell Science (2021) 134, jcs250274. doi:10.1242/jcs.250274

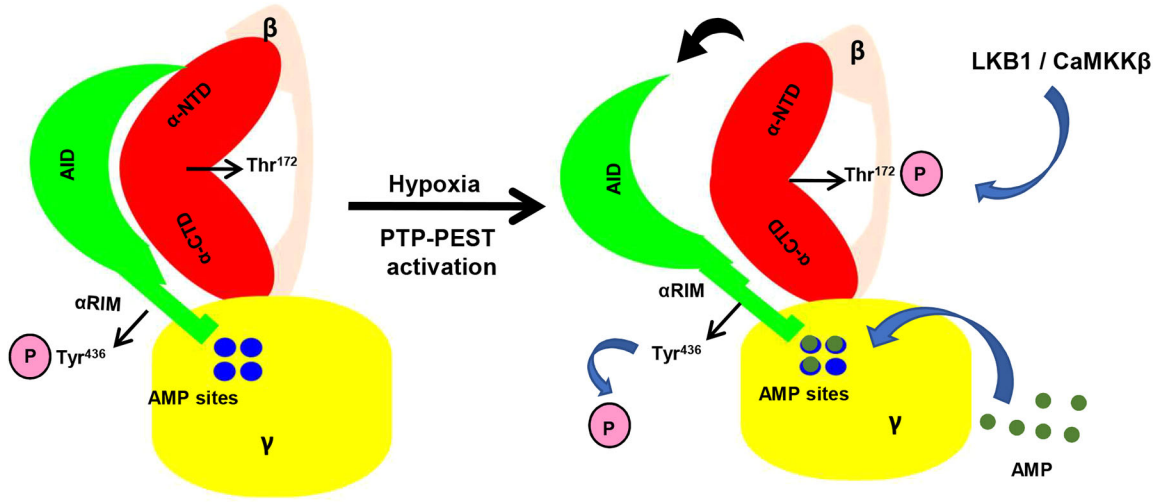

Fig. 7. Schematic representation of the proposed mechanism of AMPK activation by PTP-PEST. AMPK, being a heterotrimeric enzyme, consists of a catalytic α-subunit (red) and two regulatory subunits – β (cream) and γ (yellow). The catalytic cleft formed by the N- and C-terminal lobes (α-NTD and α-CTD, respectively) of the kinase domain (KD) of the α-subunit harbours Thr^{172}. During normoxia, the auto-inhibitory domain (AID, green), which is connected to the flexible α-RIM, binds to the back end of the KD and keeps the enzyme in an inactive state by not allowing upstream kinases such as LKB1 or CaMKKβ to phosphorylate (P) Thr^{172}. Dephosphorylation of putative tyrosine residues of AMPK by PTP-PEST during hypoxia, such as the Tyr^{436} present in the flexible and disordered α-RIM, could allow transmission of a conformational change to the connected AID, thereby dissociating it from the KD. Pulling back of the AID as a consequence of tyrosine dephosphorylation could relieve auto-inhibition and facilitate accessibility of Thr^{172} for phosphorylation by LKB1 or CaMKKβ. Additionally, due to an increase in the AMP:ATP ratio during hypoxia, AMP molecules would bind to the allosteric sites in the γ subunit to mediate allosteric activation of AMPK.

et al., 2013; Toton et al., 2018; Zhao et al., 2018). Thus, the current findings identify a hitherto unreported role of PTP-PEST in regulating endothelial autophagy via activation of AMPK.

PTP-PEST is an efficient enzyme with a K_{cat}/K_m greater than 7×10^6 M^{-1} s^{-1} (Li et al., 2016; Selner et al., 2014). A key finding of the current study is that hypoxia increases both expression and activity of PTP-PEST. It is presently unclear how hypoxia brings about these effects, but a preliminary CONSITE-based *in silico* analysis of the putative promoter region of PTP-PEST indicates presence of multiple HIF-1α binding sites (data not shown), suggesting a possible increase in PTP-PEST transcription in response to hypoxia. Alternatively, hypoxia may enhance the protein stability of PTP-PEST. A great deal is known about the ability of the 'PEST' sequences to regulate protein stability through interactions with ubiquitin ligases (Rechsteiner and Rogers, 1996). Posttranslational modifications of proline-rich 'PEST' sequences through phosphorylation or prolyl hydroxylation assist in these interactions (García-Alai et al., 2006; Ravid and Hochstrasser, 2008). HIF-prolyl hydroxylases (PHDs), in the presence of oxygen, hydroxylate proline residues to recruit von Hippel–Lindau (vHL) ubiquitin ligases (Strowitzki et al., 2019). However, under hypoxic conditions they fail to hydroxylate prolines and thus fail to induce protein degradation. In fact, this mode of regulation is primarily responsible for increasing the stability of HIF-1α under hypoxia. PHD2 (also known as EGLN1), a major oxygen sensor in endothelial cells, is found to be higher in the nuclear fraction during hypoxia (Berchner-Pfannschmidt et al., 2008), with nuclear localization of PHD2 being necessary for induction of its hydroxylase activity (Pientka et al., 2012). Since we observed cytoplasmic retention of PTP-PEST during hypoxia, as seen in Fig. S1A, it is possible that under hypoxic conditions, nuclear PHD2 fails to hydroxylate cytoplasmic PTP-PEST, thereby enhancing the protein stability of this phosphatase during hypoxia. The fact that we observed an increased interaction of deubiquitinase OTUB1 with PTP-PEST during hypoxia also supports the notion that hypoxia may increase stability of the PTP-PEST protein.

Increased activity of PTP-PEST could be a result of several events, including changes in subcellular localization, protein–protein interactions or even posttranslational modifications in response to hypoxia. We did not observe any change in subcellular localization of PTP-PEST in response to hypoxia. However, it is possible that PTP-PEST may undergo serine, threonine or tyrosine phosphorylation upon induction of hypoxia. Indeed phosphorylation of Ser^{39} is known to reduce the substrate specificity and activity of PTP-PEST (Lee and Rhee, 2019). Likewise, Tyr^{64}, an evolutionarily conserved residue in the 'P-Tyr-loop' of PTP-PEST is reported to be essential for its catalytic activity (Li et al., 2016). In contrast, Ser^{571} phosphorylation enhances PTP-PEST substrate binding (Zheng et al., 2011). Whether hypoxia induces phosphorylation of PTP-PEST to modulate its stability and/or activity is the subject of ongoing investigation in our laboratory.

By virtue of its ability to regulate important cellular processes such as cell adhesion and migration of numerous cell types including embryonic fibroblasts, endothelial cells, dendritic cells, T cells and macrophages, PTP-PEST plays an essential role in cardiovascular development, tissue differentiation and immune function (Lee and Rhee, 2019; Souza et al., 2012; Veillette et al., 2009). Yet the role of PTP-PEST in cancer is controversial, with some regarding it as a tumour suppressor, whereas others associate it with metastasis and tumour vasculature (Chen et al., 2018; Lee and Rhee, 2019; Zheng et al., 2011). Our observations of PTP-PEST regulating hypoxia-induced autophagy in native endothelial cells identifies a new functional role of this phosphatase in endothelial physiology. Whether this role of endothelial PTP-PEST is of consequence in tumour angiogenesis under transformed settings needs to be elucidated in future studies. In conclusion, data presented here demonstrate that hypoxia increases expression and activity of cytosolic PTP-PEST, which in turn activates AMPK to promote endothelial autophagy and angiogenesis.

MATERIALS AND METHODS

Experimental procedures involving isolation of endothelial cells from umbilical cords was approved by the IIT-Madras Institutional Ethics

Committee as per the Indian Council of Medical Research (ICMR), Government of India guidelines. These 2017 ICMR guidelines are in accordance with the Declaration of Helsinki.

Antibodies and chemicals

Tissue culture-grade plasticware was from Tarsons Products Pvt. Ltd., Kolkata, West Bengal, India. Antibodies against HIF-1α (CST #3716), phospho-AMPK (CST #2535), total AMPK (CST #2532), LC3 (CST #4108), phospho-ULK1 (Ser^{757}) (CST #6888), phospho-ULK1 (Ser^{317}) (CST #12753), total ULK1 (CST #8054), phospho-ACC (CST #11818), total ACC (CST #3676), PTP-PEST (AG10) (CST #4864), GST (CST #2622), His-Tag (CST #2365) and phospho-tyrosine (P-Tyr-102) (CST #9416) were obtained from Cell Signaling Technology, Boston, MA, USA. All the antibodies were used at recommended dilutions, as per product datasheets. Dulbecco's modified Eagle's medium (DMEM) and MCDB131 medium were purchased from HiMedia, Mumbai, Maharashtra, India, and foetal bovine serum (FBS) was from Gibco, Thermo Fisher Scientific, Waltham, MA, USA. Endothelial cell growth medium SingleQuots supplements (CC-4133) required for culture of endothelial cells were from Lonza, Basel, Switzerland. Unless specified otherwise, the rest of the molecular biology and biochemistry reagents were from Sigma, St Louis, MO, USA.

Cell culture

HUVECs were isolated from freshly collected umbilical cords by collagenase digestion. They were cultured in fibronectin-coated T25 flasks until a monolayer was formed. MCDB131 medium with endothelial growth supplements was used for culturing HUVECs. All the experiments were performed in passage one. The human aortic vascular smooth muscle cell line (T/G HA-VSMC; ATCC CRL-1999) was purchased from American Type Culture Collection (ATCC). HeLa (human cervical adenocarcinoma epithelial cell line), HEK293 (human embryonic kidney 293) and Huh7 (a hepatocyte cell line) cell lines were procured from the National Centre for Cell Science (NCCS), Pune, Maharashtra, India. All the cell lines were confirmed for no contamination before starting experiments. For cell lines HEK293, HeLa, Huh7 and HA-VSMC, cells were cultured in DMEM with 10% FBS. For hypoxia exposure, cells were incubated in a hypoxia incubator (5% CO_2, 1% O_2 and 95% relative humidity) for the specified duration. After degassing, the cell culture media used for hypoxia experiments were pre-equilibrated to the hypoxic environment for 2 h prior to the start of the experiment.

Immunoblotting

All the buffers used for washing and lysing of cells were degassed before use. Cells were washed with 1× cold phosphate-buffered saline (PBS) and lysed in buffer containing 50 mM Tris-HCl (pH 7.5), 150 mM NaCl, 1 mM EDTA, 1 mM EGTA, 1% TritonX-100, 0.1% SDS, 1% sodium deoxycholate, 1 mM PMSF and protease inhibitor cocktail from Sigma (St Louis, MO, USA), followed by sonication for 1 min (30% amplitude, 3 s on/off cycle; QSONICA Q700 sonicator). 50 µg of total protein was resolved on an 8% SDS–PAGE gel and transferred onto PVDF membrane. For western blotting involving detection of LC3 degradation, a 15% resolving gel was used. Blotted proteins were incubated with corresponding primary antibodies at 4°C overnight followed by incubation with horseradish peroxidase-conjugated secondary antibodies (Jackson ImmunoResearch, West Grove, PA, USA). Amersham ECL western blotting detection reagent (GE Healthcare Life Sciences) was used for detection. ImageJ version 1.45 (NIH, Bethesda, MD, USA) was used for densitometry analysis.

Immunoprecipitation and phosphatase assay

Cells were lysed in ice-cold buffer containing 50 mM Tris-HCl (pH 7.5), 150 mM NaCl, 1 mM EDTA, 1 mM EGTA, 1% Triton-X 100, 2.5 mM sodium pyrophosphate, 1 mM β-glycerophosphate, 1 mM sodium orthovanadate, protease inhibitor cocktail (Sigma) and phosphatase inhibitor cocktail 2 (Sigma) followed by 30 s of sonication. 300 µg of total protein was pre-cleared using protein A/G Sepharose beads for 1 h at 4°C. This was followed by overnight incubation with 3 µg PTP-PEST AG10 monoclonal antibody at 4°C. Protein–antibody complexes were pulled down using protein A/G Sepharose beads in 2× SDS sample buffer (10 mM Tris-HCl pH 6.8, 4% SDS, 0.2% Bromophenol Blue, 20% glycerol and 200 mM DTT). Specific pulldown of PTP-PEST was confirmed by employing a corresponding IgG isotype antibody as negative control. For the immunophosphatase assay, PTP-PEST elution was performed in Na-acetate phosphatase assay buffer (50 mM Na-acetate, 2 mM EDTA and 1 mM DTT, pH 5.0). The phosphatase assay was carried out in Na-acetate assay buffer at 30°C for 2 h, and 50 mM pNPP (para-nitrophenyl phosphate) was used as substrate. The reaction was stopped by addition of NaOH (final concentration of 0.45 M). The catalytic activity was determined spectrophotometrically by measuring the amount of pNP (para-nitrophenol) generated from pNPP. pNP released was quantified by measuring absorbance at 420 nm. For experiments involving pulldown of PTP-PEST from 500 µg of HUVEC lysate using a GST tag, 5 µg anti-GST antibody was used. Immunoprecipitation was carried out overnight at 4°C, followed by pulldown of protein–antibody complexes with protein A/G Sepharose beads for 2 h at 4°C.

Lentivirus production and transduction

Flag-PTP-PEST pcDNA3.1 plasmid construct was a kind gift from Dr Zhimin Lu, Department of Neuro-oncology, The University of Texas M. D. Anderson Cancer Center, Houston, USA (Zheng et al., 2011). PTP-PEST was subcloned in pENTR4-GST-6P1 (Addgene #17741) lentivirus entry vector backbone at BamH1 and XbaI restriction sites, followed by LR clonase-mediated gateway recombination into the third-generation lentivirus destination vector pLenti CMV Puro Dest (Addgene #17452). shRNA oligos (oligo 1, 5′-GATCCCACCAGAAGAATCCCAGAATCTCGAGATTCTG-GGATTCTTCTGGTGGTTTTTG-3′; and oligo 2, 5′-AGCTCAAAAAC-CACCAGAAGAATCCCAGAATCTCGAGATTCTGGGATTCTTCTG-GTGG-3′) were annealed in annealing buffer (10 mM Tris pH 8.0, 50 mM NaCl and 1 mM EDTA) and cloned in pENTR/pSUPER^{+} entry vector (Addgene #17338), which was recombined into pLenti X1 Puro DEST (Addgene #17297). These lentivirus entry and destination plasmids were a gift from Eric Campeau and Paul Kaufman, Program in Gene Function and Expression, University of Massachusetts Medical School, Worcester, USA (Campeau et al., 2009). For lentivirus production, recombined expression vectors were co-transfected with packaging plasmids pLP1, pLP2 and pVSVG (Invitrogen, Carlsbad, CA, USA) in 293T cells. Supernatant was collected 48 h and 72 h post-transfection and was concentrated through ultracentrifugation. Lentiviral transduction was performed in HUVECs (P_0) at a multiplicity of infection (MOI) of 15 in low serum (5%) endothelial growth medium at 70% confluency in the presence of polybrene (6 µg/ml) for 8 h. This was followed by a second round of transduction. 48 h post-transduction, puromycin (2 µg/ml) selection was performed for the next 3 days followed by splitting of cells for experimental treatment.

Immunofluorescence imaging

Following appropriate experimental treatments, HUVECs were washed with 1× PBS, followed by paraformaldehyde (4%) fixation for 20 min at room temperature. The cells were then made permeable with 0.25% Triton X-100 (10 min at room temperature). Cells were blocked with 5% serum in 1× PBS for an hour at room temperature, followed by overnight staining with primary antibodies at 4°C. Cells were then washed and incubated with fluorophore-conjugated secondary antibodies (Thermo Fisher Scientific, Waltham, MA, USA). Nuclei were counterstained with DAPI (1 µg/ml) for 5 min at room temperature, and images were captured using an LSM 700 Zeiss confocal microscope.

Mass spectrometry

HUVECs were transduced with N-terminal GST-tagged PTP-PEST lentiviral particles as described above. Post-transduction, the same pool of cells was split and upon reaching confluency were exposed to either normoxia or hypoxia (1% oxygen) for 24 h. GST-tagged PTP-PEST was pulled down via immunoprecipitation using GST antibody (Cell Signaling Technology, USA). Immunoprecipitated proteins were loaded on to an SDS-PAGE gel. SDS-PAGE was done in such a way that the electrophoresis run was stopped the moment the entire sample entered the resolving gel (12%). Each band, ∼5 mm in size, visible after Coommassie Blue staining was excised and used for proteomics analysis. The proteomic profiling was

performed by LC/MS/MS at the Mass Spectrometry and Proteomics Core facility of RGCB, Thiruvananthpuram, Kerala, India. Briefly, the excised gel pieces were subjected to in-gel trypsin digestion using sequence grade trypsin (Sigma), as per Shevchenko et al. (2006). The LC/MS/MS analyses of the extracted tryptic peptides were performed in a SYNAPT G2 High Definition mass spectrometer (Waters, Manchester, UK), which was connected to a nanoACQUITY UPLC chromatographic system (Waters) for the separation of peptides. The LC/MS/MS-acquired raw data was analysed by Progenesis QI for Proteomics V3.0 (NonLinear Dynamics, Waters) for protein identification using the Human protein database downloaded from UniProt.

Wound healing assay

HUVECs were cultured as a tight monolayer, and after 8 h of serum starvation a scratch was made with the aid of a 10 µl sterile micro-pipette tip, to create a wound. Immediately after wound creation, scraped cells were washed away and images were taken at the start as the '0 hour' time point. HUVECs were then incubated in the presence of 5 mM hydroxyurea (anti-proliferative molecule) for the next 24 h, either in normoxia or hypoxia (1% oxygen) conditions, and images were retaken at the same locations following incubation to assess migration. The area of wound closure in 24 h was calculated using ImageJ software.

In vitro tube formation assay

Wells in a 96-well plate were coated with 80 µl of growth factor free Matrigel and allowed to polymerize in a CO_2 cell culture incubator. Following appropriate experimental treatment (PTP-PEST knockdown), 15×10^3 HUVECs (with or without PTP-PEST knockdown) were seeded onto each Matrigel-coated well in low serum (1% FBS) endothelial growth medium (MCDB131) and incubated for 16 h under normoxia or hypoxia (1% oxygen) followed by imaging. Tube networks were analysed using the Angioanalyser feature of ImageJ.

Site directed mutagenesis

Sequence encoding the N-terminal 300 amino acids of wild-type PTP-PEST was PCR amplified (forward primer, 5′-CGCGGATCCATGGAGCAAG-TGGAGATC-3′; reverse primer, 5′-CCGCTCGAGTCATAGTTGTAGC-TGTTTTTC-3′) and cloned in Novagen-pET28a(+) bacterial expression vector (Merck Millipore Sigma, Burlington, MA, USA) between BamH1 and Xho1 restriction sites. Site directed mutagenesis was carried out to generate the C231S mutant using the following primers: forward primer, 5′-TGTATTCATTCCAGTGCAGGCTG-3′; and reverse primer, 5′-CAGCC-TGCACTGGAATGAATACA-3′. PCR was performed using 10 ng of His tagged PTP-PEST (WT) plasmid as template, and this was followed by Dpn1 (New England Biolabs, UK) digestion for 2 h at 37°C. The Dpn1-digested PCR product was transformed into *E. coli* DH5α ultra-competent cells. Positive clones were selected by kanamycin resistance and grown overnight in Luria Bertani (LB) broth with 0.1 mg/ml kanamycin. These constructs encode the first 300 amino acids along with an additional hexa-histidine tag at the N-terminal end. The sequences of the constructs (WT and C231S) were confirmed using DNA sequencing.

Protein expression and purification

E. coli strain BL21 codon plus RIL (DE3) harboring the relevant plasmid was grown overnight at 37°C in LB broth medium supplemented with kanamycin (0.1 mg/ml) and chloramphenicol (0.034 mg/ml). 1% of this overnight culture was transferred into fresh medium with kanamycin and chloramphenicol and grown until a cell density equivalent to an OD_{600} of 0.6 was reached. Protein expression was induced with a final concentration of 1 mM IPTG for 6 h at 30°C. Cells were then harvested by centrifugation at 4500 ***g*** for 10 min at 4°C, washed with milli-Q water and frozen at −20°C. Overexpressed proteins were purified using immobilized metal affinity chromatography (IMAC) based on the affinity of the hexa-histidine tag for Ni^{2+} following cell lysis in lysis buffer (50 mM Tris-HCl, 200 mM NaCl, 1 mM PMSF, pH 8.0). All subsequent steps were performed at 4°C. Cell lysis was achieved through sonication performed thrice for 5 min with a pulse of 5 s 'on' and 5 s 'off', at 30% amplitude. The lysate was centrifuged at 4500 ***g*** for 30 min at 4°C. The supernatant was then applied to a Ni^{2+}-NTA (nickel-nitrilotriacetic acid) Sepharose column (GE Healthcare, USA) pre-equilibrated with the lysis buffer at a flow rate of 0.2 ml/min. The protein was eluted in 50 mM Tris-HCl, 200 mM NaCl and 300 mM imidazole (pH 8.0). The fractions containing the eluted protein were pooled and immediately subjected to buffer exchange using a HiPrep 26/10 desalting column on an AKTA FPLC purification system (GE Healthcare, USA) into storage buffer (50 mM Tris-HCl, 200 mM NaCl, pH 8.0). The protein was concentrated using Amicon Ultra-15 centrifugal filter units (Millipore, Germany) to around 8 mg/ml. Size-exclusion chromatography was performed at 4°C using a HiLoad Superdex 200 pg 16/600 GE preparative column (GE Healthcare, USA). The column was equilibrated with 50 mM Tris-HCl, 200 mM NaCl, pH 8.0. Total protein (250 µg) was loaded into the column and eluted at a rate of 0.5 ml/min. The chromatograms were calibrated with the absorption of the following proteins at 280 nm: ferritin (440 kDa), aldolase (158 kDa), conalbumin (75 kDa), ovalbumin (44 kDa) and ribonuclease A (13.7 kDa). Overexpression and purification of PTP-PEST was confirmed through SDS-PAGE and size exclusion chromatography, respectively (Fig. S2A–C). Size exclusion chromatography confirmed that the purified PTP-PEST eluted as a monomeric protein. Protein concentration estimations were performed using Bradford's assay with bovine serum albumin serving as a standard.

Statistical analysis

All experimental data are represented as mean±s.e.m. for a minimum of three independent experiments. Statistical evaluation was performed using Student's *t*-test (two tailed), using GraphPad Prism version 6.0 software for Windows (GraphPad Prism Software Inc. San Diego, CA, USA). A P-value<0.05 was considered to be statistically significant.

Acknowledgements

Authors thank Dr S. Umadevi of the Translational Research Platform for Veterinary Biologicals, Tamil Nadu Veterinary and Animal Sciences University, Chennai for her technical assistance with confocal microscopy.

Competing interests

The authors declare no competing or financial interests.

Author contributions

Conceptualization: S.C., M.D.; Methodology: S.C., N. Mehta, A.A.N., R.K.T., S.B.M.; Formal analysis: S.C., A.M.; Investigation: S.C., N. Mehta, A.A.N., M.C.; Resources: M.D.; Writing - original draft: S.C., M.D.; Writing - review & editing: M.D.; Supervision: A.J., N. Manoj, M.D.; Project administration: M.D.; Funding acquisition: M.D.

Funding

This work was supported through the Department of Biotechnology, Ministry of Science and Technology, India (DBT; BT/PR12547/MED/30/1456/2014) and the Science and Engineering Research Board (SERB; EMR/2015/000704), Government of India sponsored research funding.

Supplementary information

Supplementary information available online at
https://jcs.biologists.org/lookup/doi/10.1242/jcs.250274.supplemental

Peer review history

The peer review history is available online at
https://jcs.biologists.org/lookup/doi/10.1242/jcs.250274.reviewer-comments.pdf

References

Alers, S., Loffler, A. S., Wesselborg, S. and Stork, B. (2012). Role of AMPK-mTOR-Ulk1/2 in the regulation of autophagy: cross talk, shortcuts, and feedbacks. *Mol. Cell Biol.* **32**, 2-11. doi:10.1128/MCB.06159-11

Ashraf, Q. M., Haider, S. H., Katsetos, C. D., Delivoria-Papadopoulos, M. and Mishra, O. (2004). Nitric oxide-mediated alterations of protein tyrosine phosphatase activity and expression during hypoxia in the cerebral cortex of newborn piglets. *Neurosci. Lett.* **362**, 108-112. doi:10.1016/j.neulet.2004.02.069

Bakhashab, S., Ahmed, F., Schulten, H.-J., Ahmed, F. W., Glanville, M., Al-Qahtani, M. H. and Weaver, J. U. (2018). Proangiogenic effect of metformin in endothelial cells is via upregulation of VEGFR1/2 and their signaling under hyperglycemia-hypoxia. *Int. J. Mol. Sci.* **19**, 293. doi:10.3390/ijms19010293

Barr, A. J., Ugochukwu, E., Lee, W. H., King, O. N. F., Filippakopoulos, P., Alfano, I., Savitsky, P., Burgess-Brown, N. A., Müller, S. and Knapp, S. (2009).

Large-scale structural analysis of the classical human protein tyrosine phosphatome. *Cell* **136**, 352-363. doi:10.1016/j.cell.2008.11.038

Berchner-Pfannschmidt, U., Tug, S., Trinidad, B., Oehme, F., Yamac, H., Wotzlaw, C., Flamme, I. and Fandrey, J. (2008). Nuclear oxygen sensing: induction of endogenous prolyl-hydroxylase 2 activity by hypoxia and nitric oxide. *J. Biol. Chem.* **283**, 31745-31753. doi:10.1074/jbc.M804390200

Calabrese, M. F., Rajamohan, F., Harris, M. S., Caspers, N. L., Magyar, R., Withka, J. M., Wang, H., Borzilleri, K. A., Sahasrabudhe, P. V., Hoth, L. R. et al. (2014). Structural basis for AMPK activation: natural and synthetic ligands regulate kinase activity from opposite poles by different molecular mechanisms. *Structure* **22**, 1161-1172. doi:10.1016/j.str.2014.06.009

Campeau, E., Ruhl, V. E., Rodier, F., Smith, C. L., Rahmberg, B. L., Fuss, J. O., Campisi, J., Yaswen, P., Cooper, P. K. and Kaufman, P. D. (2009). A versatile viral system for expression and depletion of proteins in mammalian cells. *PLoS ONE* **4**, e6529. doi:10.1371/journal.pone.0006529

Chen, L., Jiao, Z.-H., Zheng, L.-S., Zhang, Y.-Y., Xie, S.-T., Wang, Z.-X. and Wu, J.-W. (2009). Structural insight into the autoinhibition mechanism of AMP-activated protein kinase. *Nature* **459**, 1146-1149. doi:10.1038/nature08075

Chen, Z., Morales, J. E., Guerrero, P. A., Sun, H. and McCarty, J. H. (2018). PTPN12/PTP-PEST regulates phosphorylation-dependent ubiquitination and stability of focal adhesion substrates in invasive glioblastoma cells. *Cancer Res.* **78**, 3809-3822. doi:10.1158/0008-5472.CAN-18-0085

Davidson, D. and Veillette, A. (2001). PTP-PEST, a scaffold protein tyrosine phosphatase, negatively regulates lymphocyte activation by targeting a unique set of substrates. *EMBO J.* **20**, 3414-3426. doi:10.1093/emboj/20.13.3414

Davis, B. J., Xie, Z., Viollet, B. and Zou, M.-H. (2006). Activation of the AMP-activated kinase by antidiabetes drug metformin stimulates nitric oxide synthesis in vivo by promoting the association of heat shock protein 90 and endothelial nitric oxide synthase. *Diabetes* **55**, 496-505. doi:10.2337/diabetes.55.02.06.db05-1064

De Meyer, G. R. Y., Grootaert, M. O. J., Michiels, C. F., Kurdi, A., Schrijvers, D. M. and Martinet, W. (2015). Autophagy in vascular disease. *Circ. Res.* **116**, 468-479. doi:10.1161/CIRCRESAHA.116.303804

Dong, H., Zonta, F., Wang, S., Song, K., He, X., He, M., Nie, Y. and Li, S. (2017). Structure and molecular dynamics simulations of protein tyrosine phosphatase non-receptor 12 provide insights into the catalytic mechanism of the enzyme. *Int. J. Mol. Sci.* **19**, 60. doi:10.3390/ijms19010060

Du, J., Teng, R.-J., Guan, T., Eis, A., Kaul, S., Konduri, G. G. and Shi, Y. (2012). Role of autophagy in angiogenesis in aortic endothelial cells. *Am. J. Physiol. Cell Physiol.* **302**, C383-C391. doi:10.1152/ajpcell.00164.2011

Duffy, E. A., Pretorius, P. R., Lerach, S., Lohr, J. L., Hirsch, B., Souza, C. M., Veillette, A. and Schimmenti, L. A. (2015). Mosaic partial deletion of PTPN12 in a child with interrupted aortic arch type A. *Am. J. Med. Genet. A* **167**, 2674-2683. doi:10.1002/ajmg.a.37279

Dunwoodie, S. L. (2009). The role of hypoxia in development of the Mammalian embryo. *Dev. Cell* **17**, 755-773. doi:10.1016/j.devcel.2009.11.008

Filippi, I., Saltarella, I., Aldinucci, C., Carraro, F., Ria, R., Vacca, A. and Naldini, A. (2018). Different adaptive responses to hypoxia in normal and multiple myeloma endothelial cells. *Cell. Physiol. Biochem.* **46**, 203-212. doi:10.1159/000488423

Forsythe, J. A., Jiang, B. H., Iyer, N. V., Agani, F., Leung, S. W., Koos, R. D. and Semenza, G. L. (1996). Activation of vascular endothelial growth factor gene transcription by hypoxia-inducible factor 1. *Mol. Cell Biol.* **16**, 4604-4613. doi:10.1128/MCB.16.9.4604

García-Alai, M. M., Gallo, M., Salame, M., Wetzler, D. E., McBride, A. A., Paci, M., Cicero, D. O. and de Prat-Gay, G. (2006). Molecular basis for phosphorylation-dependent, PEST-mediated protein turnover. *Structure* **14**, 309-319. doi:10.1016/j.str.2005.11.012

Hawley, S. A., Pan, D. A., Mustard, K. J., Ross, L., Bain, J., Edelman, A. M., Frenguelli, B. G. and Hardie, D. G. (2005). Calmodulin-dependent protein kinase kinase-β is an alternative upstream kinase for AMP-activated protein kinase. *Cell Metab.* **2**, 9-19. doi:10.1016/j.cmet.2005.05.009

Jeon, S.-M. (2016). Regulation and function of AMPK in physiology and diseases. *Exp. Mol. Med.* **48**, e245. doi:10.1038/emm.2016.81

Jiang, F. (2016). Autophagy in vascular endothelial cells. *Clin. Exp. Pharmacol. Physiol* **43**, 1021-1028. doi:10.1111/1440-1681.12649

Jin, Q., Cheng, J., Liu, Y., Wu, J., Wang, X., Wei, S., Zhou, X., Qin, Z., Jia, J. and Zhen, X. (2014). Improvement of functional recovery by chronic metformin treatment is associated with enhanced alternative activation of microglia/macrophages and increased angiogenesis and neurogenesis following experimental stroke. *Brain Behav. Immun.* **40**, 131-142. doi:10.1016/j.bbi.2014.03.003

Kim, J., Kundu, M., Viollet, B. and Guan, K.-L. (2011). AMPK and mTOR regulate autophagy through direct phosphorylation of Ulk1. *Nat. Cell Biol.* **13**, 132-141. doi:10.1038/ncb2152

Koziel, A. and Jarmuszkiewicz, W. (2017). Hypoxia and aerobic metabolism adaptations of human endothelial cells. *Pflugers Arch.* **469**, 815-827. doi:10.1007/s00424-017-1935-9

Krock, B. L., Skuli, N. and Simon, M. C. (2011). Hypoxia-induced angiogenesis: good and evil. *Genes Cancer* **2**, 1117-1133. doi:10.1177/1947601911423654

Lakshmanan, A. P., Samuel, S. M., Triggle, C. H. R. I., Tuana, B. S. and Ding, H. O. N. G. (2016). A role for Sarcolemmal Membrane-Associated Protein (SLMAP) in mediating autophagy in endothelial cells through an AMPK-dependent mechanism. *FASEB J.* **30**, 948.

Lee, C. and Rhee, I. (2019). Important roles of protein tyrosine phosphatase PTPN12 in tumor progression. *Pharmacol. Res.* **144**, 73-78. doi:10.1016/j.phrs.2019.04.011

Li, H., Yang, F., Liu, C., Xiao, P., Xu, Y., Liang, Z., Liu, C., Wang, H., Wang, W., Zheng, W. et al. (2016). Crystal Structure and Substrate Specificity of PTPN12. *Cell Rep.* **15**, 1345-1358. doi:10.1016/j.celrep.2016.04.016

Li, J., Li, S., Wang, F. and Xin, F. (2017). Structural and biochemical insights into the allosteric activation mechanism of AMP-activated protein kinase. *Chem. Biol. Drug Des* **89**, 663-669. doi:10.1111/cbdd.12897

Liang, P., Jiang, B., Li, Y., Liu, Z., Zhang, P., Zhang, M., Huang, X. and Xiao, X. (2018). Autophagy promotes angiogenesis via AMPK/Akt/mTOR signaling during the recovery of heat-denatured endothelial cells. *Cell Death. Dis.* **9**, 1152. doi:10.1038/s41419-018-1194-5

Long, Y. C. and Zierath, J. R. (2006). AMP-activated protein kinase signaling in metabolic regulation. *J. Clin. Invest* **116**, 1776-1783. doi:10.1172/JCI29044

Mochizuki, Y., Ohashi, R., Kawamura, T., Iwanari, H., Kodama, T., Naito, M. and Hamakubo, T. (2013). Phosphatidylinositol 3-phosphatase myotubularin-related protein 6 (MTMR6) is regulated by small GTPase Rab1B in the early secretory and autophagic pathways. *J. Biol. Chem.* **288**, 1009-1021. doi:10.1074/jbc.M112.395087

Montesano, R., Pepper, M. S., Belin, D., Vassalli, J.-D. and Orci, L. (1988). Induction of angiogenesis in vitro by vanadate, an inhibitor of phosphotyrosine phosphatases. *J. Cell Physiol* **134**, 460-466. doi:10.1002/jcp.1041340318

Nagata, D., Mogi, M. and Walsh, K. (2003). AMP-activated protein kinase (AMPK) signaling in endothelial cells is essential for angiogenesis in response to hypoxic stress. *J. Biol. Chem.* **278**, 31000-31006. doi:10.1074/jbc.M300643200

Nussenzweig, S. C., Verma, S. and Finkel, T. (2015). The role of autophagy in vascular biology. *Circ. Res.* **116**, 480-488. doi:10.1161/CIRCRESAHA.116.303805

Pientka, F. K., Hu, J., Schindler, S. G., Brix, B., Thiel, A., Johren, O., Fandrey, J., Berchner-Pfannschmidt, U. and Depping, R. (2012). Oxygen sensing by the prolyl-4-hydroxylase PHD2 within the nuclear compartment and the influence of compartmentalisation on HIF-1 signalling. *J. Cell Sci.* **125**, 5168-5176. doi:10.1242/jcs.109041

Rankin, E. B., Rha, J., Unger, T. L., Wu, C. H., Shutt, H. P., Johnson, R. S., Simon, M. C., Keith, B. and Haase, V. H. (2008). Hypoxia-inducible factor-2 regulates vascular tumorigenesis in mice. *Oncogene* **27**, 5354-5358. doi:10.1038/onc.2008.160

Ravid, T. and Hochstrasser, M. (2008). Diversity of degradation signals in the ubiquitin-proteasome system. *Nat. Rev. Mol. Cell Biol.* **9**, 679-689. doi:10.1038/nrm2468

Rechsteiner, M. and Rogers, S. W. (1996). PEST sequences and regulation by proteolysis. *Trends Biochem. Sci.* **21**, 267-271. doi:10.1016/S0968-0004(96)10031-1

Ross, F. A., MacKintosh, C. and Hardie, D. G. (2016). AMP-activated protein kinase: a cellular energy sensor that comes in 12 flavours. *FEBS J.* **283**, 2987-3001. doi:10.1111/febs.13698

Selner, N. G., Luechapanichkul, R., Chen, X., Neel, B. G., Zhang, Z.-Y., Knapp, S., Bell, C. E. and Pei, D. (2014). Diverse levels of sequence selectivity and catalytic efficiency of protein-tyrosine phosphatases. *Biochemistry* **53**, 397-412. doi:10.1021/bi401223r

Shevchenko, A., Tomas, H., Havli, J., Olsen, J. V. and Mann, M. (2006). In-gel digestion for mass spectrometric characterization of proteins and proteomes. *Nat. Protoc.* **1**, 2856-2860. doi:10.1038/nprot.2006.468

Simon, M. C. and Keith, B. (2008). The role of oxygen availability in embryonic development and stem cell function. *Nat. Rev. Mol. Cell Biol.* **9**, 285-296. doi:10.1038/nrm2354

Sirois, J., Côté, J.-F., Charest, A., Uetani, N., Bourdeau, A., Duncan, S. A., Daniels, E. and Tremblay, M. L. (2006). Essential function of PTP-PEST during mouse embryonic vascularization, mesenchyme formation, neurogenesis and early liver development. *Mech. Dev.* **123**, 869-880. doi:10.1016/j.mod.2006.08.011

Souza, C. M., Davidson, D., Rhee, I., Gratton, J.-P., Davis, E. C. and Veillette, A. (2012). The phosphatase PTP-PEST/PTPN12 regulates endothelial cell migration and adhesion, but not permeability, and controls vascular development and embryonic viability. *J. Biol. Chem.* **287**, 43180-43190. doi:10.1074/jbc.M112.387456

Stein, S. C., Woods, A., Jones, N. A., Davison, M. D. and Carling, D. (2000). The regulation of AMP-activated protein kinase by phosphorylation. *Biochem. J.* **345**, 437-443. doi:10.1042/bj3450437

Stempien-Otero, A., Karsan, A., Cornejo, C. J., Xiang, H., Eunson, T., Morrison, R. S., Kay, M., Winn, R. and Harlan, J. (1999). Mechanisms of hypoxia-induced endothelial cell death. Role of p53 in apoptosis. *J. Biol. Chem.* **274**, 8039-8045. doi:10.1074/jbc.274.12.8039

Strowitzki, M. J., Cummins, E. P. and Taylor, C. T. (2019). Protein Hydroxylation by Hypoxia-Inducible Factor (HIF) hydroxylases: unique or ubiquitous? *Cells* **8**, 384. doi:10.3390/cells8050384

Sugano, M., Tsuchida, K. and Makino, N. (2004). A protein tyrosine phosphatase inhibitor accelerates angiogenesis in a rat model of hindlimb ischemia. *J. Cardiovasc. Pharmacol.* **44**, 460-465. doi:10.1097/01.fjc.0000143275.45289.0a

Thomas, P. D., Campbell, M. J., Kejariwal, A., Mi, H., Karlak, B., Daverman, R., Diemer, K., Muruganujan, A. and Narechania, A. (2003). PANTHER: a library of protein families and subfamilies indexed by function. *Genome Res.* **13**, 2129-2141. doi:10.1101/gr.772403

Toton, E., Romaniuk, A., Konieczna, N., Hofmann, J., Barciszewski, J. and Rybczynska, M. (2018). Impact of PKCε downregulation on autophagy in glioblastoma cells. *BMC. Cancer* **18**, 185. doi:10.1186/s12885-018-4095-1

Trinkle-Mulcahy, L., Boulon, S., Lam, Y. W., Urcia, R., Boisvert, F.-M., Vandermoere, F., Morrice, N. A., Swift, S., Rothbauer, U., Leonhardt, H. et al. (2008). Identifying specific protein interaction partners using quantitative mass spectrometry and bead proteomes. *J. Cell Biol.* **183**, 223-239. doi:10.1083/jcb.200805092

Veillette, A., Rhee, I., Souza, C. M. and Davidson, D. (2009). PEST family phosphatases in immunity, autoimmunity, and autoinflammatory disorders. *Immunol. Rev.* **228**, 312-324. doi:10.1111/j.1600-065X.2008.00747.x

Venna, V. R., Li, J., Hammond, M. D., Mancini, N. S. and McCullough, L. D. (2014). Chronic metformin treatment improves post-stroke angiogenesis and recovery after experimental stroke. *Eur. J. Neurosci.* **39**, 2129-2138. doi:10.1111/ejn.12556

Woods, A., Johnstone, S. R., Dickerson, K., Leiper, F. C., Fryer, L. G. D., Neumann, D., Schlattner, U., Wallimann, T., Carlson, M. and Carling, D. (2003). LKB1 is the upstream kinase in the AMP-activated protein kinase cascade. *Curr. Biol.* **13**, 2004-2008. doi:10.1016/j.cub.2003.10.031

Xie, Y., You, S. J., Zhang, Y. L., Han, Q., Cao, Y. J., Xu, X. S., Yang, Y. P., Li, J. and Liu, C. F. (2011). Protective role of autophagy in AGE-induced early injury of human vascular endothelial cells. *Mol. Med. Rep.* **4**, 459-464.

Yamada, E., Okada, S., Bastie, C. C., Vatish, M., Nakajima, Y., Shibusawa, R., Ozawa, A., Pessin, J. E. and Yamada, M. (2016). Fyn phosphorylates AMPK to inhibit AMPK activity and AMP-dependent activation of autophagy. *Oncotarget* **7**, 74612-74629. doi:10.18632/oncotarget.11916

Yang, C.-F., Chen, Y.-Y., Singh, J. P., Hsu, S.-F., Liu, Y.-W., Yang, C.-Y., Chang, C.-W., Chen, S.-N., Shih, R.-H., Hsu, S.-T. D. et al. (2020). Targeting protein tyrosine phosphatase PTP-PEST (PTPN12) for therapeutic intervention in acute myocardial infarction. *Cardiovasc. Res.* **116**, 1032-1046. doi:10.1093/cvr/cvz165

Zhao, L., Wang, X., Yu, Y., Deng, L., Chen, L., Peng, X., Jiao, C., Gao, G., Tan, X., Pan, W. et al. (2018). OTUB1 protein suppresses mTOR complex 1 (mTORC1) activity by deubiquitinating the mTORC1 inhibitor DEPTOR. *J. Biol. Chem.* **293**, 4883-4892. doi:10.1074/jbc.M117.809533

Zheng, Y., Yang, W., Xia, Y., Hawke, D., Liu, D. X. and Lu, Z. (2011). Ras-induced and extracellular signal-regulated kinase 1 and 2 phosphorylation-dependent isomerization of protein tyrosine phosphatase (PTP)-PEST by PIN1 promotes FAK dephosphorylation by PTP-PEST. *Mol. Cell Biol.* **31**, 4258-4269. doi:10.1128/MCB.05547-11